Citric acid-based carbon dots and their application in energy conversion

Lorenzo Vallan[*1] and Hiroshi Imahori*[*1,2]*

1) Department of Molecular Engineering, Graduate School of Engineering, Kyoto University, Nishikyo-ku, Kyoto 615-8510, Japan. E-mail: vallan.lorenzo@gmail.com; imahori@scl.kyoto-u.ac.jp

2) Institute for Integrated Cell-Material Sciences (WPI-iCeMS), Kyoto University, Sakyo-ku, Kyoto 606-8501, Japan

KEYWORDS carbon dot, citric acid, fluorophore, light emitting diode, photocatalysis, solar cell

ABSTRACT Carbon dot (CD) is a general term that encompasses a plethora of organic materials obtained from different reagents and different synthetic routes. Beyond this variety, carbonization has been considered for long time as the essential process whereby completely different precursors converge into the formation of nano-sized particles with resembling optical properties. In particular, CDs outstanding fluorescence emission is frequently attributed to the existence of large aromatic structures with extended conjugation. Nevertheless, thanks to the contribution of an increasing number of publications, nowadays the impact of these structures on the fluorescence emission has been considerably downsized. In some cases, their existence is even highly questionable. In return, in these years more solid interpretations have been provided, according to

which the chemical and emissive nature of CDs is strictly specific to the combination of synthetic precursors employed. Moreover, researchers have become more aware of the complexity of these systems, which contain not only nanoparticles, but also single molecules, oligomers and aggregates with their own fluorescent behavior. Therefore, we dedicate the first part of this review to the individual examination of different classes of citric acid-based CDs as benchmarking CDs class. A classification based on the precursors is meant to help the reader to find a common thread between CDs structural and optical properties. In the second part, we discuss the employment of citric acid-based CDs for energy conversion applications. This includes their exploitation as components of light emitting diodes (LEDs), as photocatalysts for hydrogen generation and pollutants degradation as well as additives in several types of organic photovoltaic devices.

1. INTRODUCTION

Classification of CDs

Carbon dots (CDs) are a class of organic nanoparticles exhibiting amazing fluorescence properties. Low cost and easy to prepare, water soluble and non-toxic, CDs emerged in the last decade as an excellent alternative to conventional dyes, metal-organic complexes and semiconductor quantum dots (QDs). Their optical and electronic properties have been exploited for countless analytical,[1] biomedical[2] and energy conversion applications, such as photocatalysis, light emitting diodes and solar cells.[3–5] Despite their consistent employment, the chemical nature of CDs and its relationship with their outstanding fluorescence emission are still a topic under debate, being the actual knowledge incomplete and at times contradictory. A first obstacle to the subject understanding is given by the inconsistent and misused CDs terminology, since similar or identical materials have been reported with different names, such as carbon dots, carbon

nanodots (CNDs), carbon quantum dots (CQDs), C-Dots and polymer dots (PDs). This problem has been addressed by Cayuela et al., who proposed a simple nomenclature based on the structure of the nanoparticle: CQDs are characterized by the presence of a crystalline (graphite-like) core, while the structure of CNDs is carbonized but amorphous.[6] In addition, according to Xia et al., polymeric nanoparticles with a certain degree of carbonization should be called carbonized polymer dots (CPDs), in order to distinguish them from CNDs, which are completely carbonized, and from PDs, which are purely polymeric (Figure 1).[7]

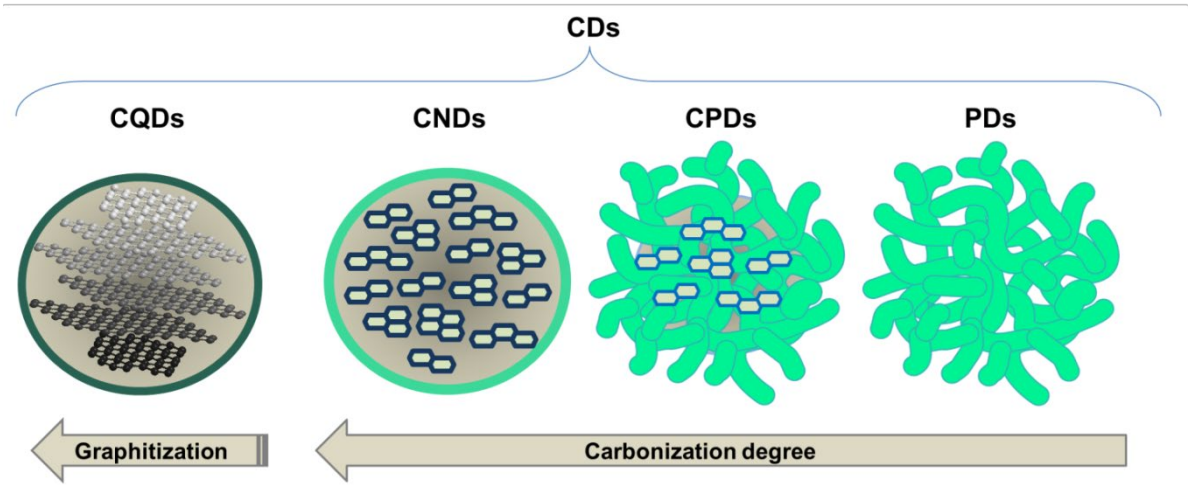

Figure 1. Schematic representation of the CDs nomenclature based on their carbonization/graphitization degree.

A meaningful name assignation is essential for enriching the bibliography with consistent data, since the understanding of the CDs optical properties is based in the first place on the fluorophore structure identification. Nevertheless, even the above-mentioned nomenclature can be sometimes equivocal. In first place, the "dot" term is confusing itself, since it was originally borrowed from the field of semiconductor quantum dots, a class of inorganic nanoparticles with 0-dimensional nature and in which the energy of the quantized states is depending on the

nanoparticle size. In reality, the fluorescence emission of CDs prepared from organic precursors has rarely shown size correlation. On the contrary, anisotropic electronic transitions have been reported for several CDs systems, implying that these objects are not 0-dimensional.[8–11] Secondly, this classification focuses on the degree of carbonization or graphitization of the nanoparticles, thus highlighting the importance of these features over other parameters. Nevertheless, several studies reported that the presence of carbonized or graphitized structures is not responsible mainly for the CDs optical properties. In some cases it is even detrimental, while polymer structures, polymer-bonded molecular fluorophores or aggregates of molecular fluorophores have a much stronger impact on the fluorescence. Therefore, at the time of understanding the structure/fluorescence relationship of specific CDs systems, a categorization based uniquely on their content of carbonized/graphitic structure could be misleading. Instead, the type of precursors employed for the CDs preparation is a more informative criterion for classification, since their resulting optical properties are heavily defined by this choice. As proposed by Zeng et al., the use of a nomenclature based both on the precursors choice and on the degree of carbonization would be highly desirable.[12] With these premises, in this review nanoparticles obtained from different precursors have been dealt separately. In particular, we decided to focus on the subcategories of CDs derived from citric acid (**CA-CDs**), being possibly the most represented CDs system in the literature.[13] Alone or, most commonly, in combination with nitrogen-containing compounds, citric acid can produce a variety of fluorescent materials with different structures and optical properties. In particular, urea, ethylenediamine (and similar aliphatic amines), aromatic bis-amines and formamide have been frequently exploited as citric acid coreactants. Recently, a short review focusing on the relationship between optical properties and synthetic conditions of CA-CDs has been published, but the influence of the precursors was

not addressed in detail.[13] Conversely, in the first part of this review each CDs system arising from specific combinations of precursors is described individually and in depth. In this way, we provide the reader with a complete and coherent picture of the structural and optical features of each system. In the second part, energy conversion applications of CA-CDs are described. Specifically, their use as photocatalysts, light emitting diodes and solar cell components over the last decade is presented. In line with the purpose of the review, also in this second part the importance of synthetic conditions and precursors on the final CA-CDs properties is discussed.

2. GENERAL ASPECTS OF CA-CDs

Synthesis – typical procedures for the synthesis of CA-CDs involve pyrolysis, hydrothermal treatment, solvothermal treatment or microwave irradiation of the molecular precursors. As the simplest procedure, pyrolysis consists of heating citric acid, alone or mixed with a coreactant, in absence of solvent (Figure 2a). The pyrolysis duration can range from few minutes to days[14,15] and the temperatures are typically comprised between 180°C, at which the thermal decomposition of CA starts, and 250°C. Higher temperatures were also reported, including completely carbonized CA-CDs at 1000°C.[16] The hydrothermal method requires the preparation of an aqueous solution of the precursors, which is transferred inside a Teflon-lined sealed autoclave and placed in an oven (Figure 2a). This method allows reaching high temperatures in a water environment, which would not be possible at atmospheric pressure. Furthermore, the protocol is highly controllable and reproducible. Temperatures between 140 and 250°C are commonly chosen and different reaction times, from one to several hours, can afford in some cases different structures.[17,18] In the solvothermal treatment, water is replaced with another solvent, such as ethanol,[19] glycerol,[20] formamide[21] or DMF,[22] chosen for improving the reagents solubility but also affecting the resulting CA-CDs structure and properties. As a drawback, the

hydrothermal/solvothermal treatment requires high energy consumption and relatively long reaction times. In contrast, microwave irradiation provides a quick and green procedure for the CA-CDs preparation. In here, a solution of the reagents is heated by irradiation in a laboratory microwave or in a domestic one (Figure 2b). Laboratory microwave allows controlling parameters such as temperature and power cycling; moreover it can work both in close- and open-vessel conditions. On the other hand, domestic microwave can be very practical, as it has access to higher radiation power and allows customizable set-up. Typically, the solution is placed in a beaker inside the domestic microwave and during the irradiation the water evaporates leaving a sticky solid. At that point, the temperature rises considerably and CA-CDs are forming. Unfortunately, this approach is not easily reproducible and the temperature reached is unknown. Other ways of producing CA-CDs have been reported, such as heating in oil bath,[23,24] sonication[25] or solar irradiation.[26]

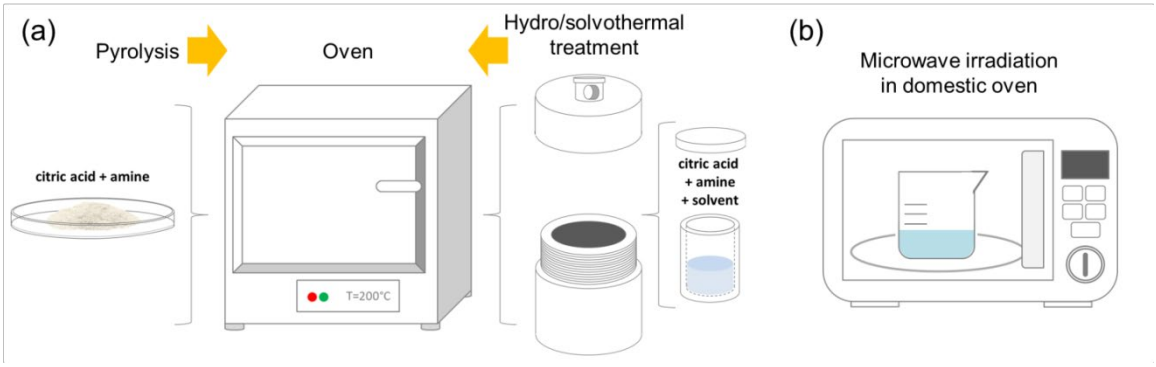

Figure 2. Schematic representation of common methods for the synthesis of CA-CDs. a) Pyrolysis and hydrothermal/solvothermal treatment. b) Irradiation in domestic microwave oven.

Purification – in spite of several reports and meta-analysis raising concerns on the problem, purification was and still remains the Achilles heel of the majority of CDs studies, including CA-CDs. According to Essner et al., from a sampling of over 550 CDs papers 12% does not report

any purification method, while another 20% employs only centrifugation or bulk filtration (Figure 3a).[27] It is clear that these procedures do not allow the removal of the molecular precursors nor of other molecules and oligomers produced abundantly from any bottom-up synthetic procedure. A more suitable method is the dialysis in water, which is the preferred option for CA-CDs purification (Figure 3b). Nevertheless, the details about this procedure are not always mentioned. Furthermore, it was demonstrated that several days of dialysis with frequent changes of water are needed in order to remove completely the molecular impurities;[27,28] conditions that are seldom respected in practice. In addition, the removal by dialysis of molecular species that are not completely soluble in water, such as some aromatic compounds, can be challenging. For example, many molecules identified among the unpurified CA-CDs mixtures form aggregates, slowing down the purification process. On the other hand, these aggregates could correspond to the CA-CDs themselves, as pointed out in several studies, thus dialysis would not be the best option for their purification.[9,29–31] Beside dialysis, chromatography techniques provide a useful approach for understanding the composition of the raw CDs. Silica column chromatography,[32–34] C18 reverse phase chromatography,[29,35] gel permeation chromatography,[36,37] size-exclusion chromatography[38] and ion exchange chromatography[39] were exploited for the purification and/or characterization of the fluorophores for various CA-CDs systems. Naturally, the efficiency of each of these methods strictly depends on the size and/or chemical nature of the individual components. In turn, those are determined by the precursors choice and the synthesis conditions; therefore it is not possible to establish a single purification method valid for all the types of CDs. On the contrary, the purification should be optimized each time depending on the system studied.

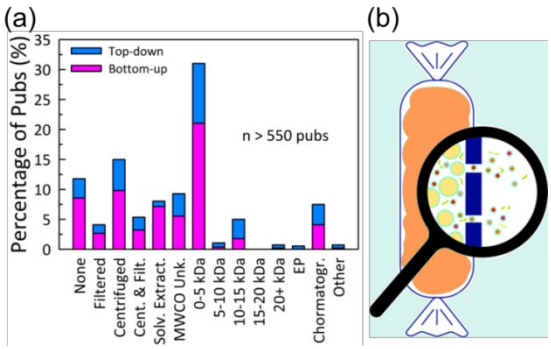

Figure 3. a) A sampling of over 550 CDs publications categorized by their mode of purification. Reproduced from ref.[27] Copyright 2018, American Chemical Society. b) Representation of dialysis purification.

Characterization – basic routine characterization of CDs involves, but is not limited to, microscopy techniques such as atomic force microscopy (AFM) and high-resolution transmission electron microscopy (HR-TEM), and spectroscopy techniques such as infrared spectroscopy (IR), X-ray photoelectron spectroscopy (XPS), UV/vis and fluorescence spectroscopy. Therefore, absent or incomplete purification can be problematic for the real understanding of the CDs structure and optical properties. The results obtained from characterization techniques like IR, XPS and elemental analysis are meaningless if large amounts of molecular species are present in the sample. In addition, since these species are frequently much more fluorescent than the CDs themselves, also the optical characterization is misinterpreted.[27] An evaluation of the sample purity can be performed by nuclear magnetic resonance (NMR) spectroscopy, a powerful and commonly available tool in chemistry laboratories. NMR techniques easily allow to spot and identify the molecular impurities. Furthermore, in some studies it provided precious information for understanding the origin of the fluorescence for different CA-CDs system.[35,40–42] Unfortunately, the employment of NMR in the CDs field is still very limited. On the contrary,

numerous studies claim the identification of graphite-like crystalline structures in CDs by means of HR-TEM and X-ray diffraction spectroscopy (XRD) characterization. In some cases, the presence of G and D bands in Raman spectroscopy is also proposed as a proof of the existence of graphite structures, even though these bands could be related to much smaller aromatic molecules.[43] Other studies suggested instead that the nanoparticles showing lattice fringes in TEM are more simply nanocrystals of polymers or aggregated organic molecules rather than graphitic cores.[44–47] This alternative interpretation sounds legitimate, especially knowing that the processes exploited for the graphite production from organic compounds require temperatures comprised between 500 and 2000°C and the use of metal catalysts.[48] Thus, it would be quite surprising if the thermal treatment of citric acid, without any catalyst and at temperatures below 200°C, leaded to such advertised "graphitic nanoparticles".

3. CA-CDs CLASSES

3.1 Carbon Dots produced from citric acid in absence of N-sources

Several types of CDs produced from the thermal treatment of only citric acid (oCA-CDs) have been reported. In a typical pyrolysis procedure, citric acid crystals are heated at 180-200°C in air, causing their melting and thermal decomposition.[14,49–51] The material shifts from colorless to orange in the process. Alternatively, the irradiation of a citric acid aqueous solution with a domestic microwave or its hydrothermal treatment has been performed.[15,28,52] In many cases, the as-produced material is dissolved in water and neutralized by addition of NaOH, without performing any purification. Information about the synthesis conditions, purification, nanoparticle size and optical properties of several types of oCA-CDs are listed in Table 1.

Table 1. Synthesis and properties of oCA-CDs.

Synthesis method	Purification	Diameter (nm)	λ_{exc}(nm)	λ_{em}(nm)	QY(%)	Ref.
Hydrothermal treatment, 180°C, 24 h, NaOH neutralization	None	-	350	440	1	.[15]
Microwave irradiation, 210°C, 10 min	Dialysis (MWCO 1 KDa)	2-3	350	450	-	.[53]
Microwave irradiation, 550 W, 7 min	Dialysis (MWCO 3.5-5 KDa)	3.2-3.8	340	440	7.2	.[52]
Pyrolysis, 160°C, 50 min, NaOH neutralization	None	2-5	360	460	29	.[54]
Pyrolysis, 180°C, 20 min, NaOH neutralization	Dialysis (MWCO 3.5-5 KDa)	0.7-1	365	460	10	.[51]
Pyrolysis, 180°C, 2 h	None	30	380	500	-	.[50]
Pyrolysis, 180°C 40 h, NaOH neutralization	None	3.5-14.3	360	460	2.6	.[55]
Pyrolysis, 180°C, 40 h, NaOH neutralization	None	4.5-9.1	360	464	2.3	.[56]
Pyrolysis, 200°C, 10 min, NaOH neutralization	Filtration and dialysis (MWCO 2 KDa)	4	355	450	0.6	.[14]
Pyrolysis, 200°C, 30 min, NaOH neutralization	None	0.6-1.1	365	450	15.4	.[57]
Pyrolysis, 200°C 30 min, NaOH neutralization	None	20	420	470	-	.[58]
Pyrolysis, 200°C 30 min, NaOH neutralization	None	2.3	365	460	-	.[59]
Pyrolysis, 200°C, 30min, NaOH neutralization	Dialysis (MWCO 3.5-5 KDa)	0.7-1	365	460	10.5	.[51]
Pyrolysis, 200°C, 30 min, NaOH neutralization	None	0.5-2	362	460	10.5	.[49]
Pyrolysis, 200°C, NaOH neutralization	None	3-7	400	470	9	.[60]
Pyrolysis, 220°C, 48 h, NaOH neutralization	Dialysis (MWCO 1 KDa)	2-7	300	385	1.2	.[15]
Pyrolysis, 260°C, 17 min, NaOH neutralization	None	-	360	460	-	.[61]
Pyrolysis, 260°C 40 min, NaOH neutralization	None	9	362	460	-	.[62]
Pyrolysis, 260°C, 50 min, NaOH neutralization	None	-	360	460	-	.[63]
Pyrolysis, 270°C, 20 min, NaOH neutralization	Dialysis (MWCO 3.5-5 KDa)	2-10	365	460	2	.[51]

Despite the use of different synthetic conditions, common features in the structural and optical characterization suggest a strong similarity among oCA-CDs. The first and most common interpretation of these features was provided by the core-surface model. According to it, thermal activation leads to the self-assembly and intermolecular dehydroxylation of citric acid molecules, forming one or more crystalline layers that constitute the nanoparticle core, while all around oxygen groups such as carboxylic acids and hydroxyl groups constitute the oCA-CDs surface (Figure 4a).[49,51,52,64] The crystalline nature of the oCA-CDs core has been frequently inferred by HR-TEM, XRD or Raman analysis. In some cases, HR-TEM images show clear lattice fringes, where the inter-layer distance resembles the graphite crystal phase,[51,64] but more commonly these features are not observable.[14,49,50,65] XRD patterns also allow calculating the interlayer distance, which is not always matching with the graphite one. Leaning on the core-surface model,

Dhenadhayalan et al. interpreted the absorption spectrum of oCA-CDs derived from the microwave-assisted pyrolysis of citric acid (550 W, domestic oven).[52] The strong absorption below 300 nm was attributed to the promotion of electrons from the valence band to the conduction band of the polyaromatic oCA-CDs core. Instead, the absorption beyond 300 nm was related to n-π^* transitions originating from the lone pair electrons of oxygen groups located on the particle surface (Figure 4b). The finding of an isoemissive point at 464 nm by means of time-resolved area normalized emission spectrum (TRANES) analysis supported the existence of two distinct emissive surface states in addition to the weakly emitting core. Nevertheless, the contribution of the core to the whole fluorescence emission is controversial, since several studies indicated as detrimental the excessive carbonization of the nanoparticles (Figure 4c).[49,51,54] In particular, Bagheri et al. performed a systematic study on the oCA-CDs formed by pyrolysis of citric acid, determining the influence of temperature and time on the QY (Figure 4d). It was shown that the best QY (29%) is reached at 160°C for 50 minutes, a significantly lower temperature than in most of the previous works. This QY record was attributed to the optimum surface passivation of the oCA-CDs, made possible by the incomplete carbonization of citric acid molecules, as well as by carboxyl and hydroxyl groups on the edges. More recently, the effective amount of graphitized structures and their impact on the fluorescence properties was further questioned. In the work of Wyrzykowski et al., the thermal behavior of citric acid was studied by thermogravimetry (TGA) and differential scanning calorimetry (DSC). According to this study, citric acid melts at 161°C and above 175°C it converts into several products, including *trans*-aconitic anhydride, itaconic anhydride and citraconic anhydride (Figure 4e).[66] Innocenzi et al. investigated the presence of these citric acid derivatives as potential intermediates of the oCA-CDs formation.[50] Citric acid monohydrate was heated at 180°C for 120 minutes, and

samples were taken from the reaction every 15 minutes once the crystals were completely molten. Infrared characterization of the samples showed that citric acid, once completely lost the adsorbed water, undergoes dehydration and decarboxylation reactions forming *trans*-aconitic acid and citraconic anhydride. Fluorescence spectroscopy studies showed that some of these oCA-CDs intermediates are blue fluorescent themselves. With the nanoparticles formation the emission maximum is red-shifted from 450 nm to 500 nm, indicating that the fluorescent species in the oCA-CDs structure are the result of the reactions between different intermediates. Moreover, by XPS estimation, it was found a C:O ratio of 1.49 after 2 h of reaction, suggesting the absence of graphene-like structures claimed instead by several previous works. These conclusions are in agreement with those of Khan and colleagues. In their work, they provided direct evidences for the formation of spherical nanocrystallites from methylene succinic acid, a molecule formed from the thermal decomposition of citric acid.[46] These nanocrystals, observable by TEM, can be easily mistaken for carbon dots with graphitic structures. In addition, the fluorophore size (0.9 nm) measured by fluorescence correlation spectroscopy does not match with the crystalline nanoparticles size measured by TEM (3.65 nm average). Therefore, rather than hypothetical CDs, the fluorophore consists of dimer or oligomers of citric acid derivatives. It is evident in this context that stricter and more efficient purification protocols are needed.

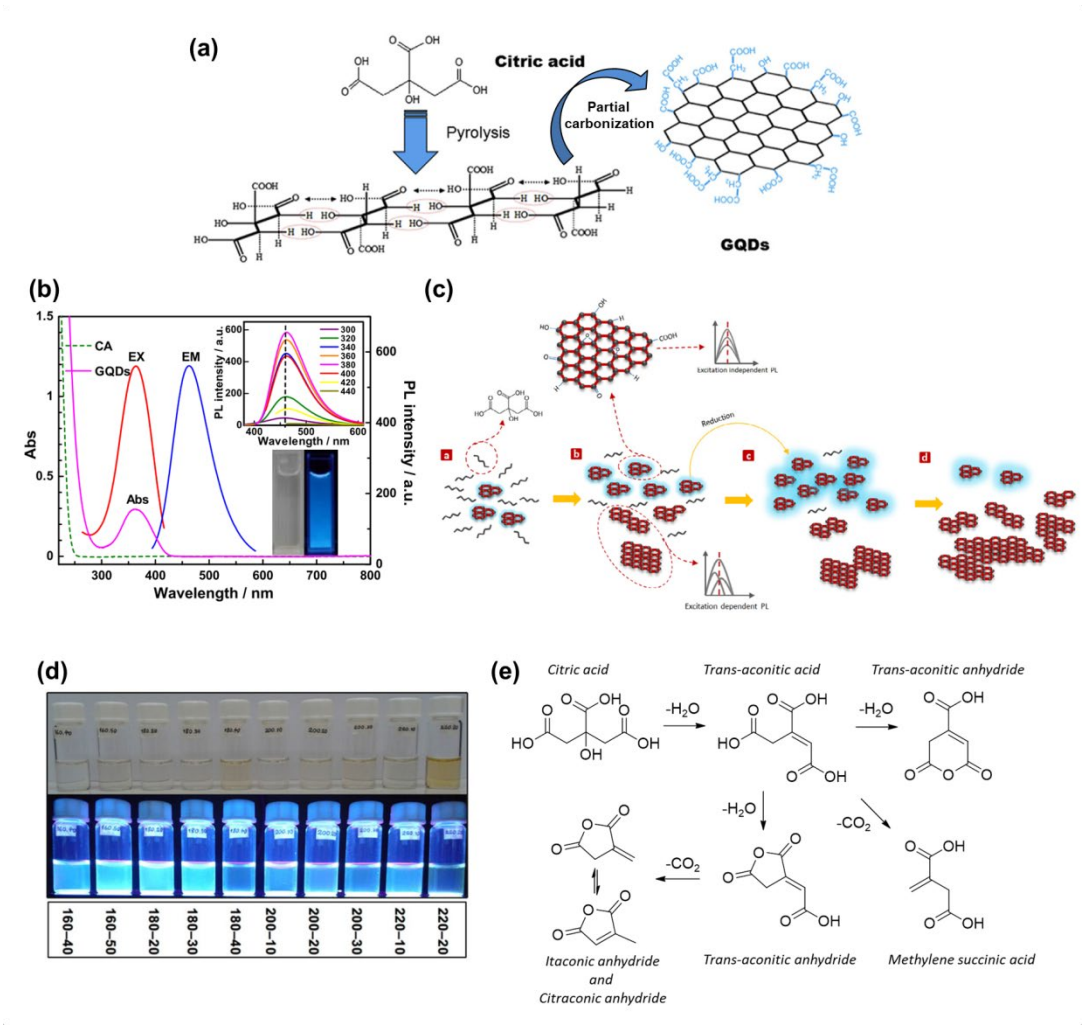

Figure 4. a) Formation of citric acid-based CDs according to ref.[49] Adapted from ref.[49] Copyright 2012, Elsevier. b) UV–vis absorption of CA and CDs, and PL spectra of CDs. Inset: (upper) emission spectra of CDs with different excitation wavelength, (lower) photographs of the CDs solution taken under visible light (left) and under 365 nm UV light (right). Reproduced from ref.[49] Copyright 2012, Elsevier. c) Schematic representation of CDs nucleation and growth according to ref.[51] Further crosslinking between CDs leads to fluorescence decrease. Adapted from ref.[51] Copyright 2015, Elsevier. d) Samples prepared at different temperatures-times under visible light and UV irradiation. Reproduced from ref.[54] Copyright 2017, Springer Nature. e) Molecules formed from the thermal decomposition of citric acid.

The complex mechanisms of citric acid thermal decomposition inevitably lead to a plethora of molecular and macromolecular structures whose role in the oCA-CDs emission has not been completely cleared. In fact, most of oCA-CDs preparation methods do not envisage an effective purification of the material. Conversely, in order to understand the real oCA-CDs contribution to the whole optical properties observed, the fraction of nano-sized material in the samples should be isolated first. The group of Chen et al. proved this point by exploiting HPLC in order to fractionate the reaction intermediates produced by citric acid thermal decomposition and isolate the oCA-CDs.[28] In this case, the raw product was obtained by the microwave-assisted irradiation (700W, domestic oven) for 7 minutes of a citric acid solution, resulting in the water evaporation and the partial carbonization of the material. The as-prepared oCA-CDs solution was filtered and then dialyzed for 120 hours (membrane MWCO=3.5 kDa). During this time, aliquots of retentate were collected and the efficiency of the purification was monitored by HPLC. Interestingly, during the dialysis process, the concentration of the retentate decreased from about 580 mg/mL to < 1 mg/mL. Thus, the nanoparticles are only a very small fraction of the whole raw material, which is mostly composed of unreacted citric acid and molecular intermediates. Clearly, long dialysis times (5 days) are required for a good purification.

3.2 Carbon Dots produced from citric acid and urea (CA/U-CDs)

Citric acid and urea are non-toxic compounds produced worldwide in large scale. Not surprisingly, they are also one of the most exploited combinations of reagents for the preparation of CDs. The synthesis can be easily performed without solvent, since the blend of citric acid and urea forms an eutectic system whose melting point is significantly lower than those of the pure compounds.[67] Typical synthesis methods are pyrolysis, hydrothermal/solvothermal treatment or microwave irradiation. As it can be observed in Table 2, the CA/U-CDs optical properties are

influenced by several parameters, such as the citric acid/urea ratio, the type, temperature and duration of thermal treatment and the purification method. In particular, the synthesis conditions choice allows targeting the prevalence of blue or of green fluorescence emission. For example, high temperatures and longer pyrolysis times cause the decrease of the absorption band with the maximum at about 350-360 nm, responsible for the blue fluorescence, and the raise of a new absorption band at about 400-420 nm, responsible for the green fluorescence (Figure 5a, 5b and 5c).[68,69] Besides, lower citric acid/urea ratios promote the green emission over the blue one (Figure 5d).[68]

Table 2. Synthesis and properties of CA/U-CDs.

CA/U ratio (mol/mol)	Synthesis method	Purification	Diameter (nm)	λ exc (nm)	λ em (nm)	QY (%)	λ exc. dependence	Ref.
0.01	Pyrolysis, 230°C, 1h	Dialysis (MWCO 3.5 kDa, 10weeks)	13.7	420	520	9	yes	[70]
0.02	Pyrolysis, 230°C, 1h	Dialysis (MWCO 3.5 kDa, 10weeks)	17.6	420	520	7	yes	[70]
0.04	Pyrolysis, 230°C, 1h	Dialysis (MWCO 3.5 kDa, 10weeks)	16.1	420	520	5	yes	[70]
0.06	Pyrolysis, 160°C, 2h	None	-	405	529	6	yes	[68]
0.31	Pyrolysis, 160°C, 2h	None	-	347	430	12	yes	[68]
0.33	Pyrolysis, 230°C, 1h	Dialysis (MWCO 3.5 kDa, 10weeks)	14	460	530	3	yes	[70]
0.94	Pyrolysis, 200°C, 2h	Centrifugation and dialysis (MWCO 0.5 kDa)	6.1	330	438	29.3	yes	[71]
0.05	Microwave irradiation, 700 W, 5 min	Centrifugation	1.1-4.5	400	522	7.5	yes	[72]
0.1	Microwave irradiation, 700 W, 5 min	Centrifugation	1.1-2.1	400	521	7.7	yes	[72]
0.16	Microwave irradiation, 650 W, 4-5 min	Centrifugation	2-20	420	540	18	yes	[73]
0.31	Microwave irradiation, 270 W, 2-3 min	Centrifugation and filtration	3-5	360	469	-	Yes	[31]
0.31	Microwave irradiation, 700 W, 5 min	Centrifugation	1.4-5.3	360	451	10.2	yes	[72]
0.31	Microwave irradiation, 700 W, 5 min	Centrifugation	23	410	540	-	yes	[74]
0.33	Microwave irradiation, 900W, 3 min	Filtration and dialysis (MWCO 3.5 kDa)	2-4	375	475	-	yes	[75]
0.94	Microwave irradiation, 700W, 5 min	Centrifugation and dialysis (MWCO 0.5 kDa)	7.3	340	433	25.1	yes	[71]
0.94	Microwave irradiation, 700W, 5 min	Centrifugation	1.7-3.1	350	419	12.1	yes	[72]
1	Microwave irradiation, 700W, 5 min	Centrifugation and filtration	16	380	520	2.1	yes	[76]
1.56	Microwave irradiation, 650W, 4-5 min	Centrifugation	4-45	360	440	15	yes	[73]
1.88	Microwave irradiation, 700W, 5 min	Centrifugation	1.3-3.5	350	420	12.2	yes	[72]
0.16	Hydrothermal treatment, 160°C, 4 h	Centrifugation	1.0-3.0	360	450	32	-	[20]
0.16	Hydrothermal treatment, 180°C, 3 h	Filtration	4.1	345	440	40	yes	[77]
0.63	Hydrothermal treatment, 180°C, 10 h	None	3-4	365	450	-	yes	[78]
0.94	Hydrothermal treatment, 200°C, 2 h	Centrifugation and dialysis (MWCO 0.5 kDa)	6.9	320	438	3.7	yes	[71]
0.1	Solvothermal treatment (DMF), 140°C, 12 h	Centrifugation and precipitation	4	360	440	52.6	yes	[18]
0.16	Solvothermal treatment (DMF), 160°C, 4 h	Centrifugation	2.0-6.0	540	600	8	-	[20]
0.16	Solvothermal treatment (DMF), 160°C, 6 h	Precipitation, redispersion and centrifugation	3.0-6.0	550	620	10.6	no	[79]
0.16	Solvothermal treatment (DMF), 180°C, 6 h	Silica column chromatography separation	2.5	365	450	19.4	no	[80]
0.16	Solvothermal treatment (DMF), 180°C, 6 h	Silica column chromatography separation	1.7	450	520	27.8	no	[80]
0.16	Solvothermal treatment (DMF), 180°C, 6 h	Silica column chromatography separation	1.8	420	550	14.6	no	[80]
0.16	Solvothermal treatment (DMF), 180°C, 6 h	Silica column chromatography separation	3.5	400	590	2	no	[80]

0.16	Solvothermal treatment (glycerol), 160°C, 4 h	Centrifugation	2.0-4.0	470	550	13		.[20]
0.3	Solvothermal treatment (DMF), 160°C, 12 h	Centrifugation and precipitation	4.1	470	540	35.1	no	.[18]
0.75	Solvothermal treatment (DMF), 200°C, 12 h	Centrifugation and precipitation	4.3	550	600	12.9	no	.[18]

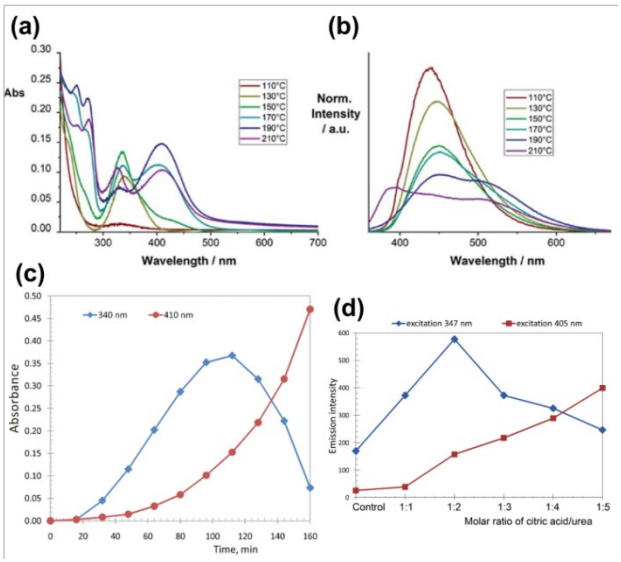

Figure 5. a) UV-vis absorption and (b) Fluorescence spectra in H_2O of selected raw products of the thermal CA/U reaction (0.013 mg/mL) at 110–210°C. c) Sequential changes in optical density at the absorption maxima of 340 nm and 410 nm of a mixture of citric acid and urea (1:5 molar ratio) upon heating at 160°C for 0–160 min. Reproduced from ref.[69] Copyright 2020, Royal Society of Chemistry. d) Luminescence intensity of the citric acid heated in the urea melt at 160°C for 120 min (aqueous solution 2 μg/mL). The x-axis is molar ratio of citric acid to urea. The control sample consisted of the products of thermal treatment of triammonium citrate (without urea) under the same conditions. Adapted from ref.[68] Copyright 2016, Beilstein Journal.

HRTEM images of CDs prepared from citric acid and urea frequently show nanoparticles with clear crystal lattice. Since the first studies, these lattice fringes have been related to the existence of sp^2 carbon domains. In parallel, the presence of aromatic nitrogen, identified by XPS analysis, has been considered responsible for the more complex fluorescent behavior and higher quantum

yields with respect to the CDs derived uniquely from citric acid.[81] According to the most widespread interpretation, citric acid thermal decomposition forms the crystalline graphite-like core through the same mechanism proposed for oCA-CDs, although, in the presence of urea, nitrogen is incorporated as dopant (Figure 6a). The term "dopant" has been adopted by countless works for defining the effect of nitrogen on the CDs optoelectronic properties, implying the occurrence of charge injection into large aromatic structures with semiconductor properties.[18,20,39,73,82–86] For example, Qu et al. obtained blue or green fluorescent CA/U-CDs using two different ratios of citric acid/urea and proposed that Fermi level energy of the conjugated sp^2 clusters can be tuned by the amount of graphitic nitrogen.[73] In recent years, this model was undermined by new investigations focusing on a more attentive separation and isolation of the fluorophores. In fact, in the majority of studies the purification procedures are inadequate if not totally absents. However, at the same time it is obvious that, beside nanoparticles, the thermal treatment of molecular precursors can produce any sort of byproduct.[27] Stachowska et al. exploited filtration or dialysis purification in order to isolate different fluorescent fractions from the raw CA/U-CDs material obtained by pyrolysis of citric acid and urea (Figure 6b).[70] The authors underline how the CA/U-CDs that have been subjected to extensive purification (10 weeks dialysis) exhibited low fluorescence emission. This is in contrast with the highly fluorescent material processed by simple filtration, thus indicating that the main contribution to both blue and green emission originates from molecular species able to permeate the dialysis membrane. The molecular dye originating the green emission was firstly identified by Kasprzyk et al.[40] In their work, the product obtained from the open-vessel microwave irradiation of citric acid and urea was placed in a dialysis membrane of MWCO=1000 Da, through which the green fluorophore is able to flow out. Thus, the green-

emitting fluorophore in the dialysate was isolated by preparative high-pressure chromatography and characterized by NMR and mass spectrometry. This allowed to identify it with the molecular structure 4-hydroxy-1H-pyrrolo[3,4-c]pyridine-1,3,6(2H,5H)-trione (HPPT, Figure 6c), of which the presence was validated by further studies.[69,87] The retentate inside the dialysis membrane revealed excitation-dependent emission, probably related to polymer chains, polymer clusters or carbon cores to which HPPT derivatives are bonded. In the same work, the microwave-assisted synthesis of CA/U-CDs in sealed-vessel condition was also performed and, in this case, blue emission was observed. According to LC-ESI-MS chromatograms, citrazinic amide was recognized as the molecular source of blue fluorescence (Figure 6c); however, other studies reached different conclusions. For example, in the work of Sendão and colleagues, CA/U-CDs synthesized by microwave treatment are purified by simple centrifugation or by extensive dialysis. In this way, it was demonstrated that the former are strongly green fluorescent and the latter are weakly blue fluorescent.[74] Therefore, blue fluorescence was attributed to CA/U-CDs nanoparticles, while green fluorescence to HPPT molecules. By means of solvent extraction and column chromatography separation, W. Strauss et al. isolated three fractions from the pyrolysis product at 230°C of citric acid and urea; namely a yellowish-brown fraction showing green emission, a colorless fraction showing blue emission and a non-fluorescent fine black powder (Figure 6d).[69] The deep structural characterization of the green fraction confirmed the previous studies by unequivocal identification of the HPPT fluorophore, while oligomeric ureas, such as triuret and cyclic tetrauret, were found in the blue fluorescent fraction. The authors suggest that strong H-bonding interactions lead HPPT and oligomeric ureas to aggregate into nanoparticles, which can further carbonize by effect of heat and form the nano-sized material found in the black powder fraction (Figure 6e). H-bonding also seems to have an important role on the formation of

aggregates in solution. In fact, it is ascertained that the optical properties of the unpurified CA/U-CDs solutions are not the simple sum of the individual fluorophores' properties.[69,74] Zholobak et al. proposed that the intramolecular forces between HPPT fluorophores and oligomeric urea drive the formation of nano-sized aggregates.[68] It was shown that the size of these aggregates strongly depends on the concentration and that the maximum emission wavelength changes as effect of the interaction with different solvents. A systematic investigation of the effect of nine polar solvents on the CA/U-CDs absorption, emission and lifetimes was performed by Anjali Devi et al.[31] The complex trends in the CA/U-CDs optical features were explained with the self-assembly of the fluorophores into different coexisting structures, i.e. H-aggregates, J-aggregates and combinations of the two, whose presence was also supported by TEM characterization.[30,31] Moreover, in the work of Bhuyan et al., it is shown how the reversible formation of aggregates from water to acetone goes in parallel with the blue emission suppression in favor of the green emission enhancement, reflecting the fluorescence resonance energy transfer (FRET)-mediated energy migration from the blue fluorophores to the green fluorophores inside the aggregate.[9] Finally, Yao et al. performed the microwave-assisted irradiation of citric acid and urea, achieving to isolate by means of reversed phase C18 column chromatography the fluorophore 5-oxopyrrolidine-3-carboxylic acid (OPCA).[29] Intriguingly, this molecule is based on a non-conjugated amide ring and it belongs to a class of emissive compounds recently named non-traditional intrinsic luminophors (NTIL),[88] i.e. organic structures that display photoluminescence in the absence of aromatic groups or metal centers. It was found that OPCA blue emission is highly enhanced by molecules aggregation, in which intermolecular interactions occur and conformational rigidity increases. Thus, in addition to the above described aromatic fluorophores, OPCA aggregation or bonding with other organic structures lies at the origin of

CA/U-CDs fluorescent emission. Similar compounds to OPCA are plausibly formed by replacing urea with aliphatic amines and they could participate to the emission of other types of CA-CDs. Therefore, further studies are necessary to assess this possibility.

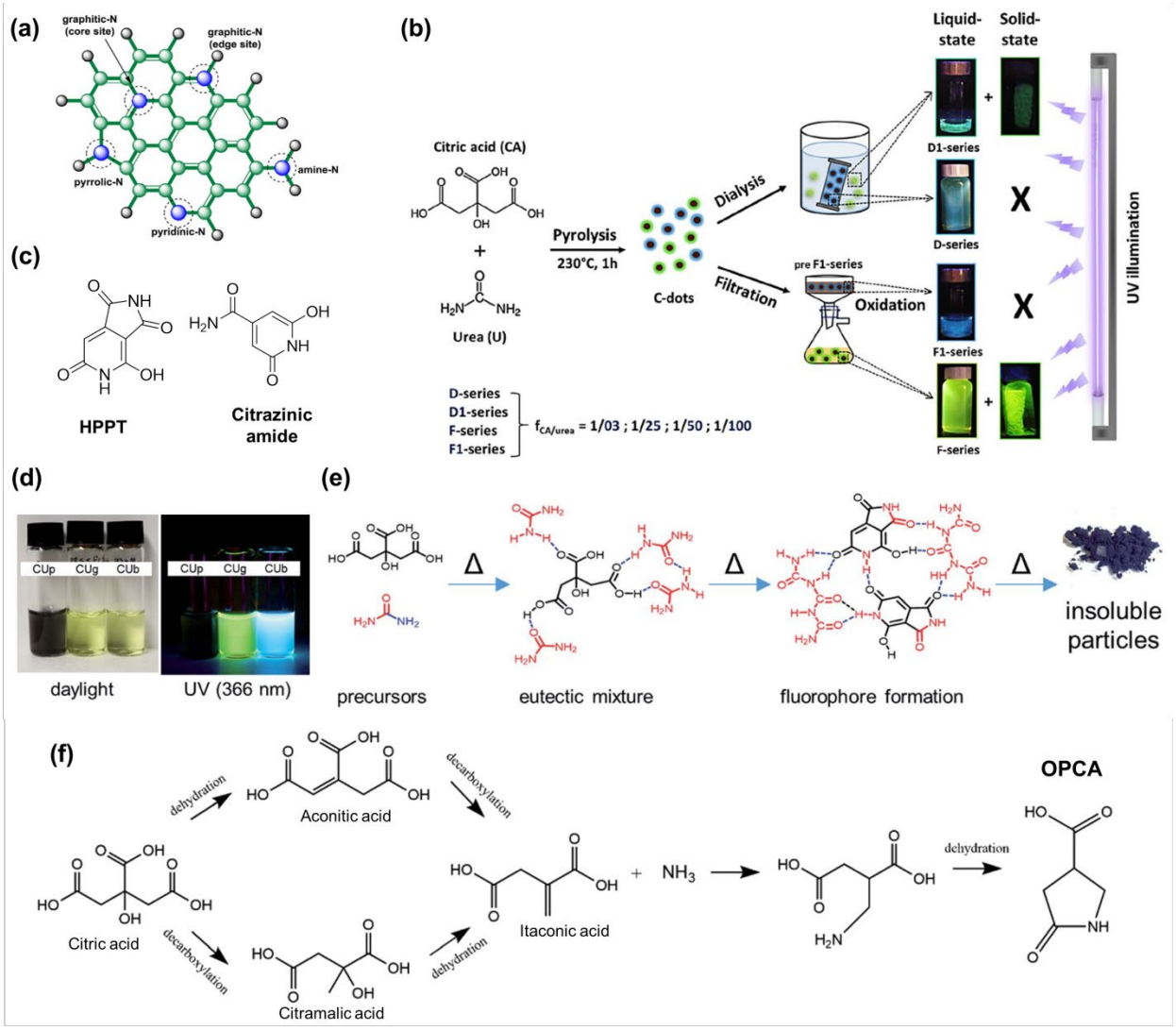

Figure 6. a) Examples of N-doping in CA/U-CDs. Green, blue and gray represent carbon, nitrogen and hydrogen atoms, respectively. Reproduced from ref.[86] Copyright 2021, Elsevier. b) Schematic representation of the synthetic and purification approach followed for the preparation of four series of photoluminescent liquids and solids, all derived by means of pyrolytic treatment of CA and urea

precursor mixtures. Reproduced from ref.[70] Copyright 2021, Springer Nature. c) Chemical structures of HPPT and citrazinic amide. d) Aqueous solutions of separated products from the crude thermal reaction product of citric acid and urea in daylight (left) and under UV light (right). e) Proposed reaction mechanism of citric acid and urea to produce solid organic nanoparticles via molecular intermediates. Reproduced from ref.[69] Copyright 2020, Royal Society of Chemistry. f) Proposed mechanism for the formation of OPCA. Reproduced from ref.[29] Copyright 2022, Royal Society of Chemistry.

As reported so far, all CA/U-CDs obtained by pyrolysis, microwave irradiation or hydrothermal treatment display blue or green fluorescent emission, which originates from individual molecular fluorophores as well as from their self-assembly into H-bonded or covalently-linked aggregates. Interestingly, CA/U-CDs with emission at longer wavelengths have been also achieved by replacing water with DMF[18,78–80,89,90] or toluene.[91] In the work of Hu et al., it is shown that the autoclave thermal treatment of 1.0 g citric acid and 2.0 g urea in 10 mL DMF can produce CA/U-CDs with tunable emission, from blue to red, by increasing the reaction temperature.[80] Similar observations are present in the work of Miao et al., who also reported that higher citric acid/urea ratios can red-shift the final CA/U-CDs emission.[18] Finally, Sun et al. demonstrated that CA/U-CDs with emission from blue to red can be obtained by increasing the reagents concentration while not changing their ratio.[89] In all these studies, the obtaining of different emission colors has been attributed to the formation of N-doped extended π-systems whose size and oxidation degree is controlled by the synthesis conditions and in turn determines the optical properties. On the other hand, this interpretation does not go along with some recently published strong evidences, according to which molecular fluorophores and aggregation dynamics are mostly responsible for originating the blue and green fluorescence of CA/U-CDs.

Furthermore, the active role of DMF in the CA/U-CDs formation has not been taken into account, even if, at the temperatures employed for their synthesis, this solvent is known for decomposing into carbon monoxide and dimethylamine and for participating to several types of reactions.[92–94] Therefore, a better understanding of the structures produced from the DMF-thermal treatment of citric acid and urea is of extreme interest for the development of long-wavelength CA/U-CDs and more studies on the subject are desirable.

3.3 Carbon Dots produced from citric acid in formamide (CA/F-CDs)

Citric acid-based CDs synthetized by formamide solvothermal treatment deserve a separate discussion as these materials, in addition to the blue and/or green emission, all share the ability to emit in the red. For example, Ding et al. obtained red fluorescent CA/F-CDs in gram scale by simply heating a citric acid and ethylenediamine mixture at 180°C for 24h in autoclave (Figure 7a).[21] The material, afforded by precipitation, displayed an excitation-independent emission at 627 nm with a record QY of 53%. In another work, citric acid and urea in formamide were heated in autoclave at 180°C for 12h and the resulting material was separated by preparative anion-exchange column to obtain fractions exhibiting blue, green, yellow or red fluorescence alone.[39] By means of XPS studies, the emission red-shift was correlated to the increasing amount of graphitic nitrogen from the blue-emissive to the red-emissive fraction. The solvothermal treatment of citric acid in formamide produces red-fluorescent CA/F-CDs even in absence of other nitrogen sources, as reported by Zhou and coworkers.[65] In any case, several studies underlined the fact that formamide not only acts as a solvent, but also participates to the CA/F-CDs formation itself or by generating other molecular species through thermal decomposition.[34,95–98] For example, the microwave-assisted irradiation of ammonium citrate in 25 mL glycerol yields blue fluorescent CDs, but, by adding first 3 mL of formamide, red

fluorescent CA/F-CDs are obtained.[99] While the above-mentioned studies related the red fluorescence to the presence of extended aromatic domains in the CA/F-CDs core, other works claimed instead its molecular origin.[35,100,101] Deng et al. performed the solvothermal treatment of citric acid and urea in formamide, adjusting the synthesis condition in order to optimize the red fluorescence emission (CA/U=0.7, 200°C, 1 h). The material was eluted on a C18 reversed-phase column. After three rounds of separation, the obtained CA/F-CDs fractions exhibited seven discrete colors under UV illumination, covering the entire visible spectrum (Figure 7b). Investigated by TEM, all the fractions showed the presence of similar amorphous nanoparticles, without evidences of crystalline structures. IR, Raman, XPS and NMR characterization jointly with spectroscopic studies and TD-DFT calculations suggested that small molecular fluorophores (MW<500 Da), either bonded or unbounded to the CA/F-CDs polymer structure, are responsible for the green and blue fluorescence. Instead, the red emission is attributed to the presence of larger molecular dyes (500-3500 Da) such as pyrene analogs. Naturally, more studies will be necessary to ascertain the exact nature of the red emitting structures, but the key-role of formamide is unquestionable: red CA/F-CDs have been obtained in formamide from citric acid with or without amine sources but also from amines in absence of citric acid.[102] It is important to notice that the thermal decomposition of pure formamide can also produce complex polymers with aromatic and nitrogen-rich structures, whose independent role has not been considered yet.[103,104]

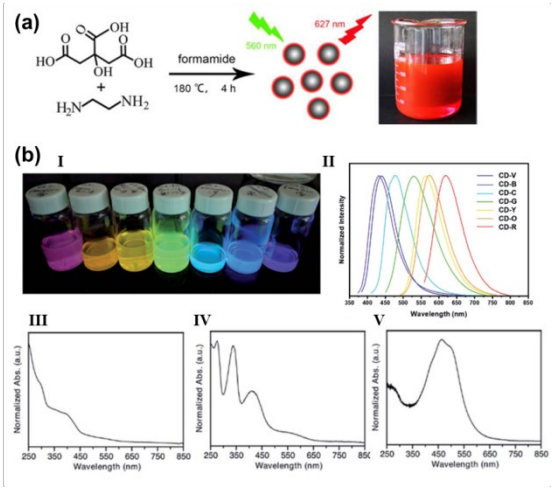

Figure 7. a) The synthetic route of the R-CDs and the product under room light. Reproduced from ref.[21] Copyright 2017, American Chemical Society. b) I. Photograph of obtained CD fractions illuminated by UV light; II. their normalized fluorescence spectra. III-V. UV-Vis extinction spectra of CD-B, CD-G, and CD-R. Reproduced from ref.[35] Copyright 2020, with permission from the Royal Society of Chemistry.

3.4 Carbon Dots produced from citric acid and ethylenediamine (CA/E-CDs) or other polyamines

Highly fluorescent, blue emissive CDs can be easily obtained by heating an aqueous solution of citric acid and ethylenediamine. As in the case of other types of citric acid-based CDs, this phenomenon was firstly attributed to the formation of carbonized cores rich of extended aromatic domains. Although still widespread, this interpretation has been eroded step by step by several in-depth analysis focused on the understanding of the CA/E-CDs structure, which has pointed out the minor or sometimes detrimental contribution of the carbonization process to the main fluorescence emission. In this framework, the work of Zhu et al. has been particularly influential. They explored the synthesis of numerous citric acid-based CDs prepared with different amine

reagents and reaction conditions.[105] Besides, they proposed a congruent mechanism for the CA/E-CDs formation. Adjusting the citric acid and ethylenediamine concentrations, a QY of 80% was reached by hydrothermal treatment. In addition, it was observed that, in a range of reaction temperatures between 150 and 300°C, a much higher QY was achieved at lower temperature (Figure 8a and 8b). Furthermore, the emission from the CA/E-CDs prepared at lower temperatures was more subjected to photobleaching with respect to the emission of CA/E-CDs prepared at higher temperatures, suggesting a major contribution from molecular fluorophores in the first case. Therefore, it was proposed that the CA/E-CDs formation occurs in two steps: first, citric acid and ethylenediamine condensate and form polymer nanoparticles bearing highly fluorescent moieties. The emission of these moieties is independent from excitation wavelength. Second, if the temperature is high enough, the partial carbonization of the polymer and the formation of a weakly fluorescent carbonized core take place at the expenses of the organic fluorophores (Figure 8c). Due to its structural heterogeneity, the emission of the core is excitation wavelength-dependent (Figure 8b). Very similar conclusions were reached by Krysmann et al. in the case of CA/E-CDs prepared from the pyrolysis of CA and EDA.[106] The authors observed that the carbonization process starts only above 230°C, while below this temperature polymeric nanoparticles and molecular fluorophores are the only products.

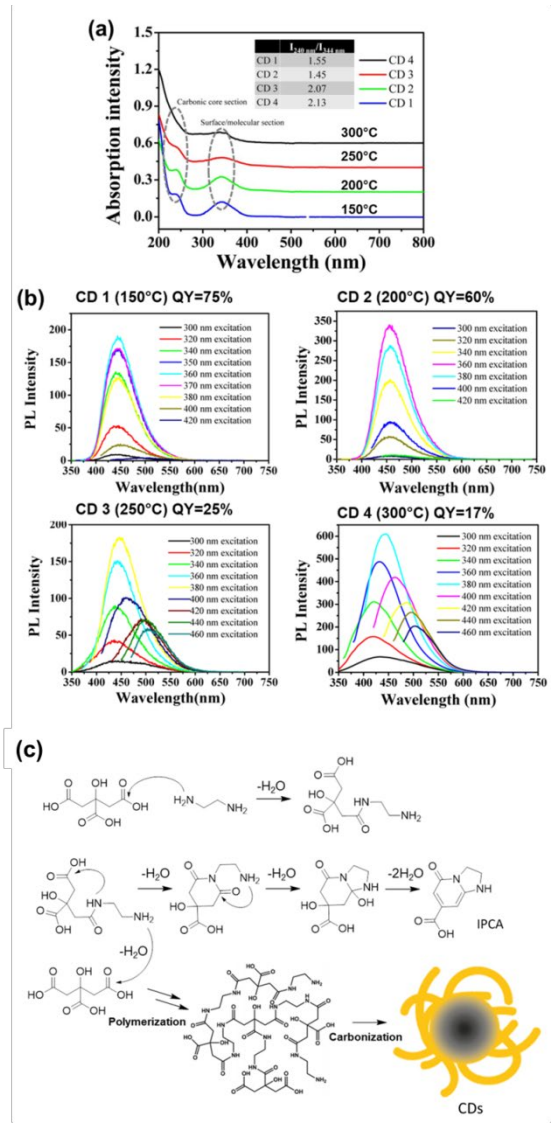

Figure 8. a) The UV-vis absorption of CD 1-4, prepared in a range of temperature between 150 and 300°C. The peak at 344 nm (surface/molecule center) decreases from CD 1 (150°C) to CD 4 (300°C), reflecting the consumption of the molecular fluorophore in favor of the carbonization process. b) The QY decreases accordingly and the emission, from excitation wavelength-independent (CD 1 and 2), becomes excitation wavelength-dependent (CD 3 and 4). Reproduced from ref.[105] Copyright 2013, Wiley-VCH.

c) Possible mechanism for the formation of IPCA fluorophores, polymer species and carbonized CA/E-CDs.

Deng et al. performed the hydrothermal treatment (200°C, 5 h) of citric acid and ethylenediamine and, by exploiting a gradient ultracentrifugation method, separated the resulting material into fractions according to the components hydrophilicity (Figure 9a and 9b).[107] Interestingly, it was found that the most carbonized particles, which are the less hydrophilic, are also the less fluorescent ones, while the purely polymeric and highly hydrophilic particles display the highest fluorescence emission (Figure 9c and 9d). It was proposed that the carbonized core is able to partially self-adsorb the fluorescence emission of the molecular state, thus acting as a quencher (Figure 9e).

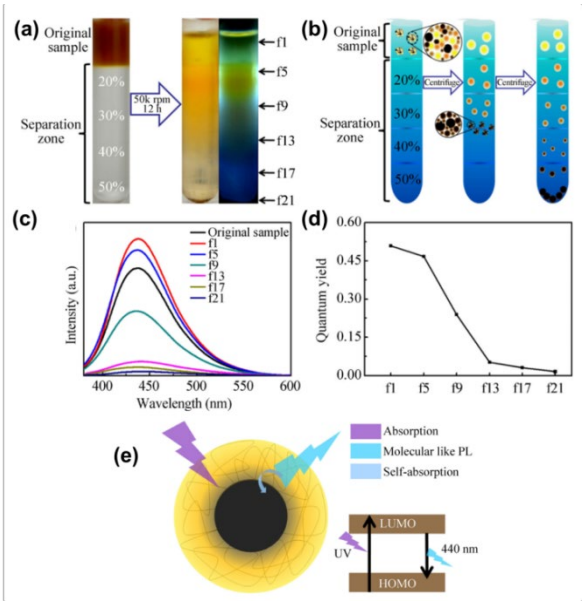

Figure 9. a) Photographs of the centrifuge tube (under ambient light) before and after centrifugation (left: under ambient light, and right: under UV light). b) Scheme of proposed mechanism of separation: CA/E-CDs were clustered at starting point and de-clustered at successive layers with increasing water content during sedimentation. c) PL spectra of original

sample and separated fractions (excited at 340 nm; all samples diluted to the same absorbance). d) QY variation of typical fractions, showing that more hydrophilic CA/E-CDs have higher fluorescence. e) Scheme of absorption, emission and re-adsorption of highly carbonized CA/E-CDs. Reproduced from ref.[107] Copyright 2015, Springer Nature.

The size and location of the organic fluorophore was further investigated by Hsu and colleagues by means of fluorescence anisotropy methods, finding that the main contribution to the whole emission originated from emitters of about 0.65 nm size, thus smaller than most of the particles observed in TEM.[11] The first identification of the molecular organic fluorophore was reported by Song et al., who fractionated the hydrothermal products (140°C, 8h) of citric acid and ethylenediamine by silica column chromatography and characterized the fluorescent fractions by NMR, mass spectrometry and elemental analysis.[41] It was found that the major responsible for the blue fluorescence was not the nanoparticles fraction, but the molecule, 5-oxo-1,2,3,5-tetrahydroimidazo[1,2-a]pyridine-8-carboxylic acid (IPCA). In addition, IPCA derivatives or other molecular emitters bonded to the CA/E-CDs core could be responsible for the more complex emissive behavior of CA/E-CDs with respect to the isolated IPCA fluorophore.[41,108] The syntheses of IPCA and similar fused 2-pyridones from citric acid and β-amines were explored in the work of Kasprzyk et al.[109] For example, by replacing ethylenediamine with cysteamine or L-cysteine, 5-oxo-3,5-dihydro-2H-thiazolo[3,2-a]pyridine-7-carboxylic acid (TPCA) and 5-oxo-3,5-dihydro-2H-thiazolo[3,2-a]pyridine-3,7- dicarboxylic acid (TPDCA) are obtained respectively, whose presence was attested in CDs prepared from these reagents.[110] The existence of defined molecular fluorophores, which can form in parallel but also take part to the polymerization process and formation of nanoparticles, is not the sole origin of the CA/E-CDs fluorescence. Besides the molecular fluorophores, at high temperature

citric acid and ethylenediamine or other polyamines undergo condensation, dehydration and crosslinking reactions that create CDs with compact and spatially constrained structures. In this circumstance, the proximity inside the CDs of electron rich groups, such as amides, amines and carboxylic acids, can force the electron-cloud overlaps and energy-level splittings without the need to form specific chemical bonds.[111] Thus, new electronic transitions become accessible and the structural rigidity of the environment, hampering the energy dissipation of the absorbed photons through rotational and vibrational motions, promotes instead the radiative relaxation of the excited state originating light emission (Figure 10).[112–114] This phenomenon was summarized in the concept of crosslink-enhanced emission (CEE) effect by Yang's group.[7,115–117]

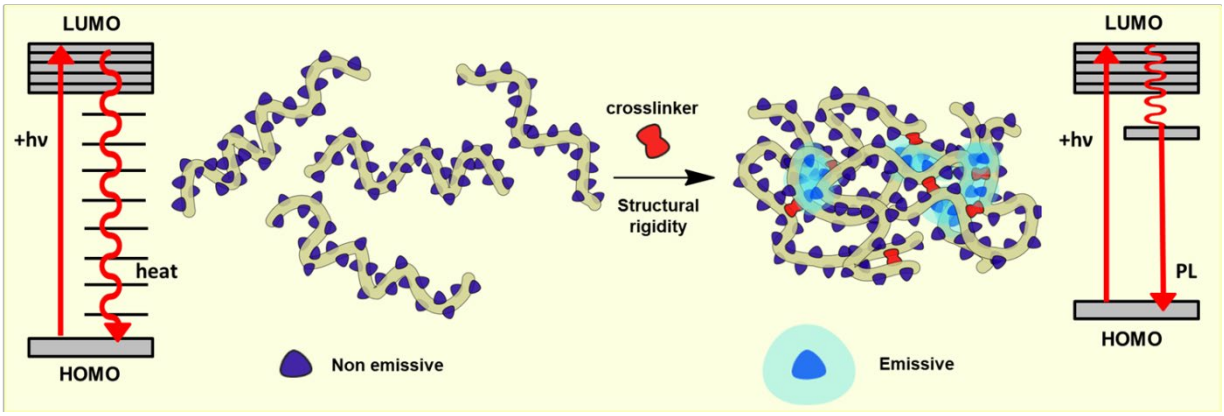

Figure 10. Graphical representation of the CEE effect. On the left, free chains of polymer carrying electron-rich groups. Upon light absorption, energy is dissipated by vibrational and rotational motions. On the right, the polymer chains are crosslinked and form a rigid bundle. Upon light absorption, vibrational relaxation is impeded and fluorescence emission occurs.

The work of Vallan et al. provided evidences of the crosslink-enhanced effect emission phenomenon in CDs derived from citric acid and ethylenediamine.[42] In here, the amidation reaction between carboxylic acids and amines was carried out by microwave irradiation (140°C,

3 min.) or by the employment of the N,N′-diisopropylcarbodiimide coupling agent at room temperature (Figure 11a). Both synthetic pathways produced polyamide nanoparticles, comparable in size and chemical structures, and no aromatic C=C double bonds were detected by NMR spectroscopy. Interestingly, both types of CA/E-CDs exhibited strong blue fluorescence, demonstrating that the polymer structure is itself emissive without the contribution of molecular conjugated fluorophores or the one of a carbonized core (Figure 11b and 11c). Amide bonds, intramolecular H-bonds and electrostatic interactions were proposed as the responsible for the high conformational rigidity promoting the CEE effect. Furthermore, CDs prepared from tricarballylic acid (without –OH group) instead of citric acid displayed much weaker emission, highlighting the role of the hydroxyl group in assisting structural rigidity (Figure 11a).

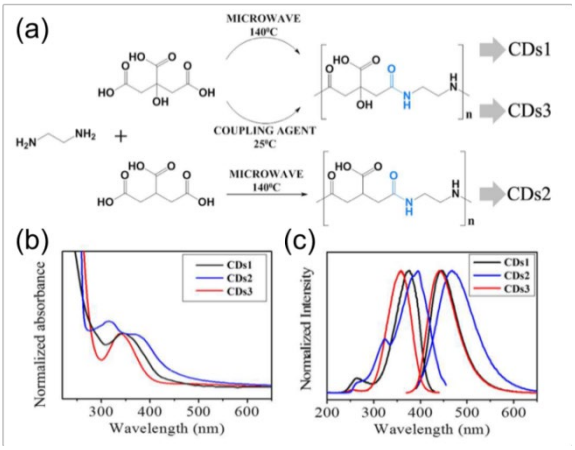

Figure 11. a) Reaction of EDA with citric acid or with tricarballylic acid to form polymeric CA-CDs by microwave irradiation or by coupling agent. b) UV/Vis, c) excitation and emission spectra of the as-produced CA-CDs. Reproduced from ref.[42] Copyright 2018, American Chemical Society.

Several types of fluorescent citric acid-based polymer dots were synthesized at room temperature by the same group, showing the versatility of the coupling agent-mediated polycondensation.[118] In fact, the CEE effect does not require specific molecules, but it is rather

common when amide (or imide) crosslinkers are present, which is a characteristic of all the CDs systems obtained from polyamine- and polycarboxylic acid-bearing precursors. For example, CDs have been prepared from citric acid with polyethyleneimine[119,120] or aminoacids;[121–123] or from polyacrylic acid with ethylenediamine.[115,124] Aromatic bis-amines have been also employed for the CDs synthesis with citric acid. In particular, phenylenediamines and diaminonaphthalenes were exploited for achieving different emission colors (Table 3). For example, several green fluorescent CDs have been prepared by hydrothermal treatment of citric acid with *p*-phenylenediamine.[25,125–127] Yuan et al. obtained five different CDs, exhibiting fluorescence from blue to red, by ethanol solvothermal treatment of 1,5-diaminonaphthalene or 2,3-diaminonaphthalene and different reaction conditions (Figure 12).[17]

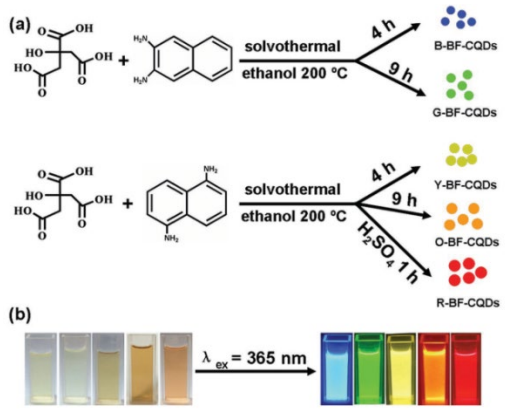

Figure 12. a) Preparation of fluorescent CDs from blue to red by solvothermal treatment of CA and 1,5- or 2,3-diaminonaphtalene. b) Photographs of the obtained CDs solutions in daylight (left) and under UV light (right). Reproduced from ref.[17] Copyright 2017, Wiley-VCH.

The emissive mechanisms behind the multicolor fluorescence of citric acid/aromatic bis-amine-based CDs have not been rationalized yet and several works attributed it to the presence of large aromatic systems or molecular fluorophores. Moreover, phenylenediamines thermal

treatment is known to produce fluorescent nanoparticles and fluorescent dyes even in absence of citric acid.[128–130]

Table 3. Synthesis and properties of CDs obtained from citric acid and aromatic polyamines.

Amine	Coreactant	Synthesis method	Purification	Diameter (nm)	λ_{exc}(nm)	λ_{em}(nm)	QY (%)	λ exc. dependance	Ref.
o-phenylenediamine	-	hydrothermal treatment, 160°C, 8 h	Centrifugation and dialysis (MWCO 0.5 kDa)	3	370	440	92	no	.[131]
o-phenylenediamine	-	hydrothermal treatment, 200°C, 5 h	Centrifugation and dialysis (MWCO 1 kDa)	1.6	370	446	49	no	.[132]
o-phenylenediamine	-	solar irradiation in a funnel-shape tin paper, 2 min	Dialysis (MWCO 0.5 kDa)	4.3	378	462	65	no	.[26]
o-phenylenediamine	-	solvothermal treatment (DMF), 200°C, 5 h	Sephadex column chromatography	3-8	400	450	46	yes	.[36]
o-phenylenediamine	-	ultrasonication, 42 kHz, 1h, argon	Filtration and size exclusion chromatography	2	400	562	-	no	.[38]
o-phenylenediamine	-	ultrasonication, 42 kHz, 1h, argon	Filtration and size exclusion chromatography	3.4	400	562	-	no	.[25]
o-phenylenediamine	-	Coupling agent-mediated polycondensation, r.t.	Filtration and dialysis (MWCO 0.5-1 kDa)	1.2	390	433	3.9	yes	.[118]
m-phenylenediamine	H_3PO_4	hydrothermal treatment, 200°C, 5 h	Centrifugation and dialysis (MWCO 1 kDa)	4.8	393	504	-	yes	.[133]
m-phenylenediamine	-	microwave irradiation, 200°C, 30 min, 300 W	Dialysis	5-7	365	430 (548 in solid)	30	yes	.[134]
m-phenylenediamine	-	Coupling agent-mediated polycondensation, r.t.	Filtration and dialysis (MWCO 0.5-1 kDa)	1.2	350	440	1.6	yes	.[118]
p-phenylenediamine	-	hydrothermal treatment, 180°C, 4 h	Filtration	2.4	360	450	-	no	.[135]
p-phenylenediamine	-	hydrothermal treatment, 200°C, 8 h	Filtration and dialysis (MWCO 0.5 kDa)	2.3	360	500	12	yes	.[125]
p-phenylenediamine	-	hydrothermal treatment, 200°C, 8 h	Dialysis (MWCO 0.5 kDa)	3.6	360	496	9	yes	.[126]
p-phenylenediamine	-	hydrothermal treatment, 210°C, 11 h	Filtration and dialysis (MWCO 0.5 kDa)	3.7	360	505	-	yes	.[127]
p-phenylenediamine	-	microwave irradiation, 800W, 50 s	Filtration	3.4	360	445	45	no	.[136]
p-phenylenediamine	-	Coupling agent-mediated polycondensation, r.t.	Filtration and dialysis (MWCO 0.5-1 kDa)	1.6	370	440	0.8	yes	.[118]
1,5-diaminonaphthalene	H_2SO_4	solvothermal treatment (EtOH), 200°C, 1 h	Dialysis	6.7	500	625	12	no	.[17]
1,5-diaminonaphthalene	-	solvothermal treatment (EtOH), 200°C, 4 h	Dialysis	3.8	420	552	58	no	.[17]
1,5-diaminonaphthalene	-	solvothermal treatment (EtOH), 200°C, 9 h	Dialysis	4.9	480	583	53	no	.[17]
2,3-diaminonaphthalene	-	solvothermal treatment (EtOH), 200°C, 4 h	Dialysis	2	360	454	75	no	.[17]
2,3-diaminonaphtalene	-	solvothermal treatment (EtOH), 200°C, 9 h	Dialysis or silica column cromatography	5	360	500	70	no	.[137]
2,3-diaminonaphthalene	-	solvothermal treatment (EtOH), 200°C, 9 h	Dialysis	2.4	380	534	73	no	.[17]

3.5 Scheme of the CA-CDs fluorophores

In summary, the thermal treatment of citric acid in combination with various nitrogen-containing sources affords a large variety of fluorescent structures. The type and fluorescent behavior of these structures mostly depends on the precursors' combination and it cannot be generalized. Thus, a simplified scheme showing the fluorescent products of the most relevant

combinations is proposed in Figure 13, in order to recapitulate the content of the previous sections.

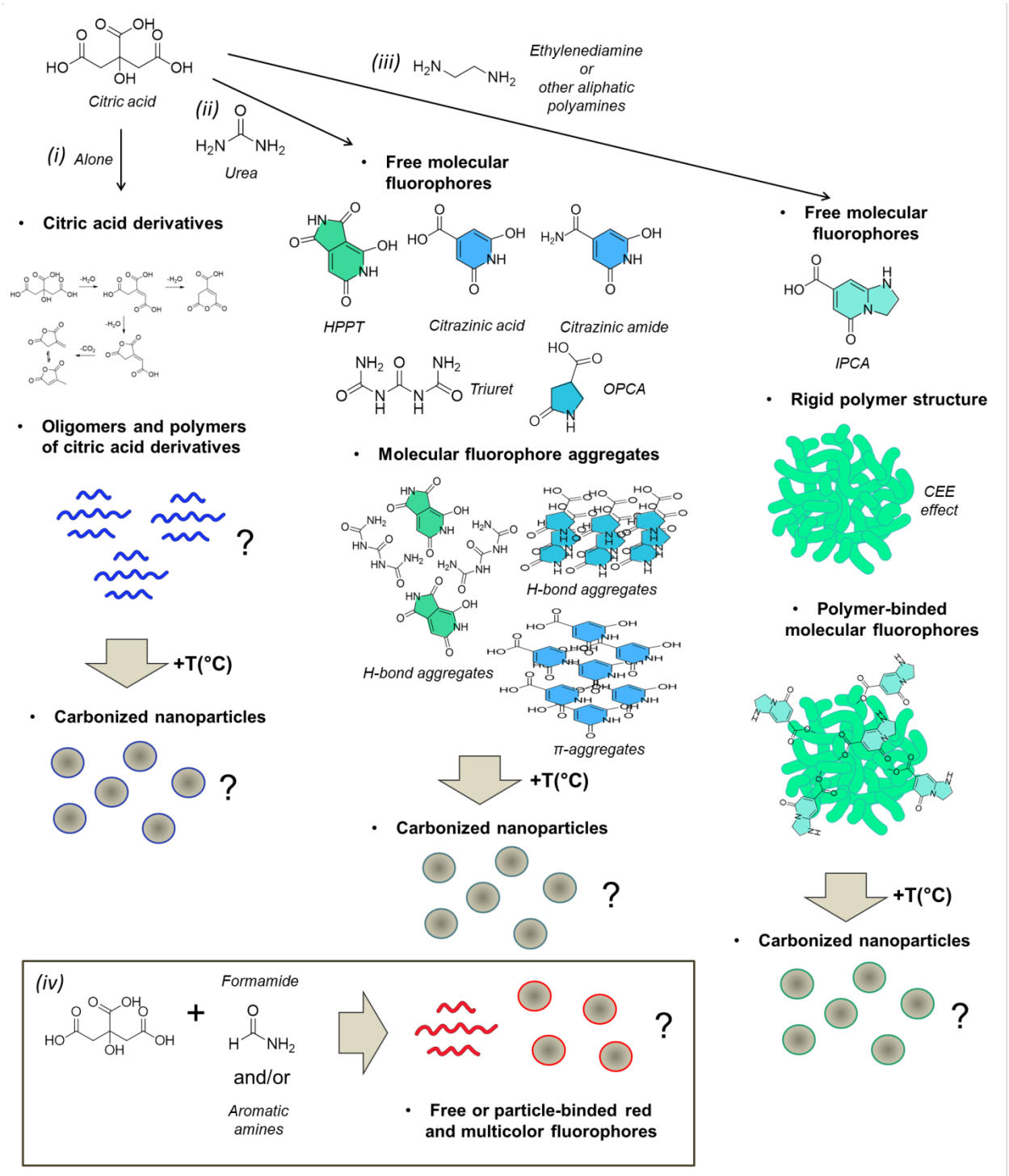

Figure 13. Simplified scheme of the fluorophores produced by thermal treatment of citric acid (i) alone, (ii) with urea, (iii) with ethylenediamine or other polyamines, (iv) with formamide. The employment of very high temperatures, normally above 200-250°C, causes a loss of oxygen by dehydration and decarboxylation reactions. Unpredictable reaction pathways bring to the formation of heterogeneous aromatic structures. The question marks indicate a lack of knowledge regarding the precise nature of these structures.

4. CA-CDs FOR ENERGY CONVERSION APPLICATIONS

Photoactive materials are at the base of numerous applications, including conversion of light into chemical transformations and into electricity or, vice versa, conversion of electricity into light. Nowadays, the seek for suitable cheap and green materials is more current than ever, also due to the advancing global energy crisis that imposes a change in the way energy is produced and consumed. Thus, the outstanding optical properties of CA-CDs motivated researcher to test their implementation in several energy conversion technologies. Even if still in its infancy, the use of CA-CDs in the energy conversion field already achieved very promising results, calling for further studies. Therefore, in the next part of this review we present the latest advances of CA-CDs in the field of light-emitting diodes, photocatalysis and solar cells, in which these materials have been largely exploited.

4.1 CA-CDs in light-emitting diodes

Low energy consumption, high current-to-light efficiency and compact design make LEDs technology extremely versatile. On the other hand, difficult manufacture and high cost of components could limit LEDs rapid diffusion and new alternatives should be searched among cheap, easy to produce and non-toxic materials. In this context, CDs-based light emitters are

extremely promising candidates. In fact, CA-CDs have been successfully employed as phosphors or as emissive layer for the preparation of LEDs. In the first case, CDs, typically embedded in a transparent polymer, form a layer that encapsulates the diode (color conversion layer): the UV light emitted from the device is absorbed by the CDs layer and converted to colored fluorescence emission (Figure 14a). In the second case, CA-CDs, alone or in a photoconductive polymer matrix, have been employed as the emissive layer of the device, where charge recombination occurs with the emission of light (Figure 14b). In the next sections, several examples of the two categories are given.

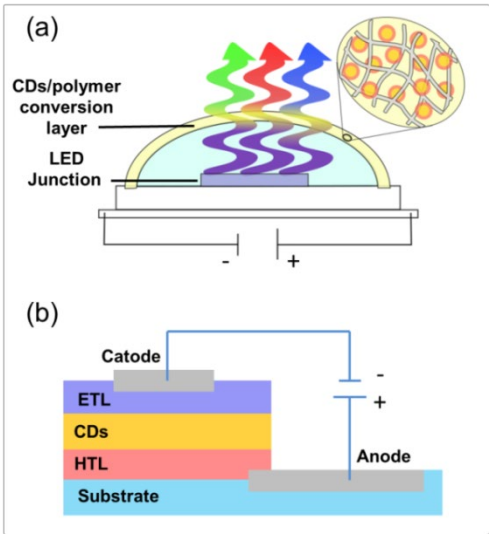

Figure 14. a) Scheme of the color conversion mechanism by CDs phosphors covering a UV-LED chip. b) Scheme of a LED structure using CDs as emissive layer. ETL and HTL represent the electron transport layer and the hole transport layer respectively. Substrate is typically glass.

In phosphor-based LEDs auto-quenching is a relevant issue that need to be addressed first, since CDs powder is typically non-emissive due to nanoparticles aggregation. Therefore, several strategies have been explored in order to obtain space-confined CDs and suppress quenching in solid. Most commonly, CDs are dispersed in polymers chosen for their hydrophilic character,

high optical transparency and good mechanical properties, such as polyvinyl alcohol (PVA),[80,138] Poly(methyl methacrylate) (PMMA),[139] Poly(2-hydroxyethyl methacrylate) (PHEMA),[140] Polyvinylpyrrolidone (PVP),[90] polyamide resin[141] and epoxy resins.[18,122,142,143] Besides, quenching resistant nanoparticles can be obtained in situ during CDs formation. Organic silanes have been broadly exploited for this purpose and several CDs-based phosphors were synthesized from the reaction between citric acid and silyl ethylenediamines.[142,144–149] The thermally-activated hydrolysis and polymerization of silyl groups produce tethered and clustered silanes, which passivate the CDs surface and prevent their aggregation.[147] Variations in the phosphor concentration or in the conversion layer thickness is an intelligent approach for tuning the chromaticity of the LEDs emission. The fluorescence emission traveling along the output path is progressively reabsorbed by other CDs, and, so higher is the CDs concentration or the path length, so more probable becomes the reabsorption of the shorter wavelengths, producing a gradual enhancement of the long wavelengths component.[149,150] This phenomenon was exploited by Zhang et al., who prepared WLEDs with only one type of CDs simply by tuning the concentration.[122] Zhou et al. prepared five LEDs with different chromaticity and color temperatures by adjusting the ratio between CDs-based phosphor and polymer matrix.[151] Several more examples of WLEDs obtained with the employment of only one CA-CD type are reported in literature (Table 4).[139,140,146,152,153]

Table 4. CA-CDs in LEDs color conversion layer.

CDs precursors	Synthesis method	Composition of the conversion layer	LED color	CIE 1931	CRI	CCT (K)	LE (lm/W)	
ammonium citrate, formamide, glycerol	Microwave irradiation, 1 min	YAG:Ce layer and CDs/SiO_2 layer in epoxy glue	White	(0.33, 0.34)	91	4962	67.5	[99]
CA and N-(3-trimethoxysilylpropyl)ethylenediamine	Microwave irradiation, 180°C, 5 min	KH-792-CDs	White	(0.32, 0.36)	-	6071	-	[142]
CA, 1-amino-2-naphthol hydrochloride	Solvothermal treatment, 180°C, 12h	Two types of CDs in OE-6550A/B silica gel	White	(0.32, 0.33)	86	5989	-	[154]
CA, 5-amino-1,10-phenanthroline	Hydrothermal treatment, 200°C, 7h	Mixture of CDs in PHEMA	White	(0.33, 0.33)	92	-	30.5	[140]
CA, ammonium hydroxide	Hydrothermal treatment, 200°C, 12h	CDs, $SrSi_2O_2N_2$:Eu and $Sr_2Si_5N_8$:Eu in epoxy resin	White	(0.33, 0.37)	95	5447	-	[155]

CA, EDA, oleylamine, HNO3	Octadecene, 250°C, argon	CDs in PMMA	Warm white	(0.37, 0.41)	-	4385	-	[139]
CA, monoethanolamine or aminoacids	Microwave irradiation	Mixture of CDs in epoxy resin	Warm white	(0.43,0.41)	96	3059	41.2	[122]
CA, monoethanolamine or aminoacids	Microwave irradiation	Mixture of CDs in epoxy resin	White	(0.33,0.36)	97	5475	46.8	[122]
CA, N-(3-Trimethoxysilylpropyl)ethylenediamine	240°C, 5min	KH-792-CDs in silicone	White	(0.30, 0.21)	74	5030	79.4	[148]
CA, N-(3-Trimethoxysilylpropyl)ethylenediamine	Hydrothermal treatment, 180°C, 4h	CDs/CdS in silicone	Yellow-white	(0.27, 0.32)	71	9051	-	[156]
CA, N-(3-Trimethoxysilylpropyl)ethylenediamine	Hydrothermal treatment, 200°C, 6h	KH-792-CDs	White	(0.29, 0.32)	84	8285	-	[145]
CA, N-(3-Trimethoxysilylpropyl)ethylenediamine	Hydrothermal treatment, 200°C, 6h	KH-792-CDs	White	(0.31, 0.36)	84	6282	-	[146]
CA, Nile blue A	Solvothermal treatment (water and/or EtOH), 200°C, 5h	Mixture of CDs in epoxy resin	White	(0.31, 0.29)	87	5643	-	[157]
CA, thiourea	Hydrothermal treatment, 160°C, 6h	CDs/YAG:Ce^{3+}/PVA	White	(0.23, 0.31)	75	7342	19.9	[158]
CA, thiourea, ammonium fluoride	Solvothermal treatment (DMF), 180°C, 8h	CDs in epoxy resin	White	(0.36, 0.36)	94	4705	-	[143]
CA, urea	Hydrothermal treatment, 180°C, 4h	Mixture of CDs in PVP	White	(0.33, 0.33)	89	5612	-	[135]
CA, urea	Microwave irradiation, 750W, 5 min	CNDs@$BaSO_4$/PDMS	White	(0.34, 0.39)	72	5002	21	[151]
CA, urea	Solvothermal treatment (DEF), 160°C, 4h	CDs in epoxy resin	Blue	(0.21, 0.54)	-	47920	63	[159]
CA, urea	Solvothermal treatment (DMAC), 160°C, 4h	CDs in epoxy resin	Warm white	(0.38, 0.49)	-	4492	22	[159]
CA, urea	Solvothermal treatment (DMF), 120, 150, 180°C, 6h	Mixture of CDs in PVA	White	(0.32, 0.33)	83	4820	-	[80]
CA, urea	Solvothermal treatment (DMF), 140-200°C, 12h	Mixture of CDs in epoxy resin	White	(0.35, 0.30)	92	5606	-	[18]
CA, urea	Solvothermal treatment (DMF), 160°C, 4h	CDs in epoxy resin	White	(0.35, 0.42)	-	5054	15	[159]
CA, urea	Solvothermal treatment (DMF), 160°C, 6h	SiO-CDs/YAG:Ce^{3+}	Warm white	(0.38,0.39)	76	4072	83.2	[160]
CA, urea	Solvothermal treatment (DMF), 180°C, 8h	CDs in PVP	White	(0.35, 0.33) or (0.394, 0.323)	80	4807	10.2	[90]
CA, urea	Solvothermal treatment (H2O, DMF or glycerol), 160°C, 4h	Na_2SiO_3/CDs in PDMS	White	(0.34, 0.31)	82	5048	8.34	[20]
CA, urea, AEPMDS, IPMDS	220°C, 30 min	CDs:AEPMDS:IPMDS	White	(0.32, 0.32)	84	12336	30	[147]
CA,N-(3-trimethoxysilylpropyl)ethylenediamine	Microwave irradiation, 180°C, 5 min	Mixture of CDs in PVA	White	(0.42, 0.41)	83	3466	-	[144]

CA-CDs as emissive layer in LEDs –Notably, the majority of CA-CDs exploited for the preparation of LEDs emissive layer are synthesized at high temperature, ranging from 250 to 300°C.[23,161–164] It is possible that a high carbonization degree is beneficial or even essential in order for CA-CDs to exhibit electroluminescence, as the presence of large aromatic domains enhances charge mobility. Another common feature of many electroluminescent CA-CDs is the presence of long aliphatic chains in their structure, which confers them oleophilic character.[23,161–165] This is a crucial requirement for the preparation of CA-CDs organic solutions and for processing them into smooth and homogeneous films. Furthermore, when CA-CDs are mixed with a photoconductive polymer, the oleophilic character allows their good dispersion in the

matrix and obviates CDs aggregation.[33,163] For example, Yuan et al. prepared the LED emissive layer by mixing CA-CDs with polyvinylcarbazole (PVK), obtaining a blue emitting device with a maximum EQE of 4%,[33] corresponding to a current efficiency of 2.6 cd A^{-1} and exceeding that of Perovskite-based deep-blue LEDs.[166–168] Instead, in the work of Zhang et al. blue, cyan, magenta and white light could be obtained by tuning the voltage of the CA-CDs-based LED.[23]

4.2 CA-CDs in photocatalysis

CA-CDs have demonstrated noteworthy photocatalytic potential for several applications, including photocatalytic hydrogen generation from water, photoreduction of carbon dioxide and photodegradation of dyes and harmful molecules. Several photocatalysts for hydrogen production were obtained by preparing CA-CDs heterojunctions with semiconductors, such as TiO_2 nanocrystals, [22] carbon nitride (g-C_3N_4) and MoS_2 nanosheets.[169] For example, Chen et al. developed a highly efficient ternary photocatalyst, constructed using Cu-In-Zn-S, CA-CDs and MoS_2. The hydrogen production rate of CIZS/MoS_2/CDs was of 3706 μmol $g^{-1}h^{-1}$, 6.65 times to that of pure CIZS and 148.24 times to that of MoS_2. According to the authors, the strong electron storage ability of CA-CDs restricted the charge recombination and enhanced the charge separation at the heterojunction interfaces (Figure 15a).[170] In the works of Zhang, photocatalytic overall water splitting has been achieved coupling CA-CDs with CuNi or of CuCo plasmonic bimetal-based photocatalysts (Figure 15b and 15c).[171,172] According to these studies, CA-CDs can accept and store electrons from the co-catalyst conductive band, facilitating the photoinduced separation of the electrons and holes and enhancing the photocatalytic ability of the composite.

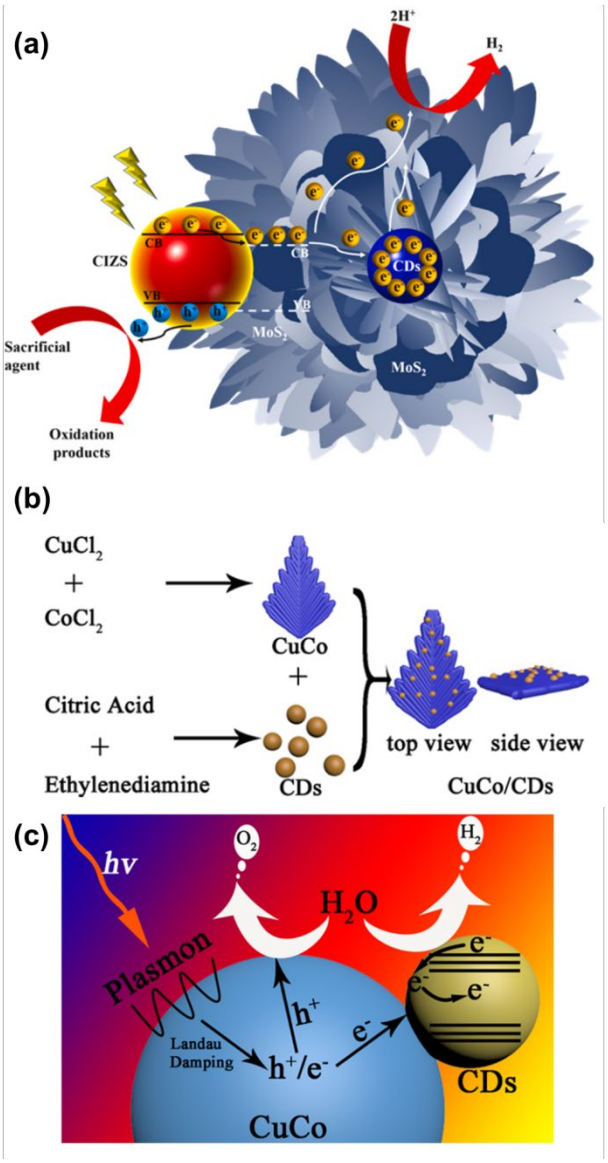

Figure 15. a) Schematic mechanism illustration for CIZS/MoS_2/CDs. Reproduced from ref.[170] Copyright 2022, Elsevier. b) Synthesis route of CuCo/CA-CDs dendrite-like structures. c) Schematic illustration of the photocatalytic overall water splitting mechanism. Reproduced from ref.[171] Copyright 2020, American Chemical Society.

Few works also reported the employment of CA-CDs photocatalysts in H_2 production in absence of cocatalyst and investigated the photocatalytic mechanism.[120,173] In particular, Jana et al. achieved record H_2 evolution rate of 19.70 mmol (H_2) g (catalyst)$^{-1}$ h^{-1} in seawater with CA-

CDs obtained by microwave irradiation of citric acid and urea (200°C for 5 min).[173] However, the as-prepared CA-CDs are not active directly, but they need to be activated by 90 minutes of Sun-simulated irradiation and air exposition. During this time, two consecutive transformations are observed in the absorption spectrum of CA-CDs (Figure Xa, b and c). It is known that nanoparticles prepared from thermal treatment of citric acid and urea contain citrazinic acid and HPPT molecular fluorophores. Thus, the authors studied the optical transformations occurring for these two molecules under the same illumination conditions and they found good match with those spectral changes seen for CA-CDs. These changes were attributed to the photoxidation, dimerization and trimerization of citrazinic acid. Furthermore, they proved that a simple mixture of citrazinic acid and HPPT also exhibits H_2 generation ability. In there, HPPT has a role in accelerating the chemical reactions occurring on citrazinic acid. Finally, the author suggested that molecular fluorophores derived from citrazinic acid are the main responsible for the CA-CDs photocatalytic ability.

Beside solar fuel production, CA-CDs photocatalytic ability has been widely exploited for the degradation of pollutants (Table 5).[174] Upon light absorption, electron transfer can occur from and to the excited CA-CDs-based material. OH^- oxidation and O_2 reduction at the photocatalyst surface produce the •OH radical and the $•O_2^-$ superoxide anion respectively, that can further react with organic pollutants. The detection of these reactive species in the CA-CDs photocatalytic media has been confirmed by several studies.[175–177]

Table 5. CA-CDs employed as photocatalysts for dyes and pollutants degradation.

CDs precursors	CDs synthesis method	Photocatalyst	Pollutant	Efficiency and time	Ref.
Ammonium citrate, EDA	Hydrothermal treatment, 200°C, 5h	CDs/OV-BiOBr	Tetracycline hydrochloride	82.7% in 60 min	.[178]
Ammonium citrate, EDA	Hydrothermal treatment, 200°C, 5h	CDs/Bi_2WO_6	Tetracycline hydrochloride	97% in 25 min	.[179]
CA	Hydrothermal treatment, 180°C, 8h	CDs/layered mesoporous TiO_2	Methyl orange	91.0% in 24 min	.[180]

CA	Pyrolysis, 200°C, 30 min	CDs/stainless-steel nanotubes	Phenanthrene	93% in 360 min	.[181]
CA	Pyrolisis, 180°C, 2h	Y-Ag_3PO_4/CDs/$BiVO_4$	Atenolol	90.9% in 360 min	.[182]
CA	Microwave irradiation (EtOH), 150°C, 5 min	CDs/WS_2 nanosheets	Congo red	12% in 10 min	.[183]
CA, (3-aminopropyl) triethoxysilane	Pyrolysis, 200°C	TiO_2/CDs nanocomposite	Methyl orange	39.1% in 120 min	.[184]
CA, ascorbic acid	Hydrothermal treatment, 160°C, 3h	CDs/α-Bi_2O_3	Levoflaxcin	79% in 120 min	.[185]
CA, ascorbic acid	Hydrothermal treatment, 160°C, 3h	CDs/α-Bi_2O_3	Indigo carmine	86% in 120 min	.[185]
CA, diethylenetriamine	Hydrothermal treatment, 200°C, 5h	CDs alone	Methylene blue	97% in 160 min	.[177]
CA, diethylenetriamine	Hydrothermal treatment, 230°C, 12h	CDs/Fe(III)	Aminopyrine	99% in 15 min	.[186]
CA, EDA	Microwave irradiation, 800W, 10 min	CDs/CdSe-rGO	Tetracycline hydrochloride	90% in 60 min	.[187]
CA, EDA	Hydrothermal treatment, 180°C, 6h	CDs/bismuth oxyiodide	Methyl orange	98% in 5 min	.[188]
CA, EDA	Hydrothermal treatment, 180°C, 5h	CDs/g-C_3N_4	Rhodamine B	95.2% in 210 min	.[189]
CA, EDA	Hydrothermal treatment, 180°C, 5h	CDs/g-C_3N_4	Tetracycline hydrochloride	78.6% in 240 min	.[189]
CA, EDA	Hydrothermal treatment, 160°C, 8h	CDs/$LaCoO_3$/ATP	Tetracycline hydrochloride	78% in 120 min	.[190]
CA, EDA	Hydrothermal treatment, 160°C, 8h	CDs/$LaCoO_3$/ATP	Chlortetracycline	46% in 120 min	.[190]
CA, EDA	Hydrothermal treatment, 240°C, 5h	CDs alone	Rhodamine B	100% in 25 min	.[175]
CA, EDA	Hydrothermal treatment, 240°C, 5h	CDs alone	Cefacrol	83% in 25 min	.[175]
CA, EDA	Hydrothermal treatment, 180°C, 5h	CDs/ZIS/BiOC	Tetracycline hydrochloride	82.3% in 60 min	.[191]
CA, L-cysteine	Hydrothermal treatment, 120°C, 5h	CDs/porous Eu micro-networks	Rhodamine 6G	95% in 160 min	.[192]
CA, L-cysteine	Hydrothermal treatment, 200°C, 6h	CDs/hollow tubular g-C_3N_4	Tetracycline hydrochloride	82.7% in 40 min	.[193]
CA, thiourea	Hydrothermal treatment, 160°C, 4h	CDs/TiO_2 P25	Rhodamine B	60% in 90 min	.[83]
CA, thiourea	Hydrothermal treatment, 180°C, 12h	CDs/TiO_2 hollow structure	Methylene blue	95% in 10 min	.[194]
CA, urea	Microwave irradiation, 5 min	CDs/Bi:TiO_2	Rhodamine B	96.4% in 40 min	.[176]
CA, urea	Microwave irradiation, 5 min	CDs/Bi:TiO_2	Phenol	92.7% in 120 min	.[176]
CA, urea	Microwave irradiation, 800W, 4 min	CDs/TiO_2	acid red 88	84% in 60 min	.[195]
CA, urea	Hydrothermal treatment, 180°C, 5h	CDs/$Bi_5Nb_3O_{15}$	Sarafloxacin	86.8% in 180 min	.[196]
CA, urea	Hydrothermal treatment, 180°C, 12h	CDs/$ZnMoO_4$	Methylene blue	99.6% in 100 min	.[197]
CA, urea	Hydrothermal treatment, 180°C, 5h	CDs/g-C_3N_4/SnO_2	Indomethacin	90.8% in 80 min	.[198]
CA, urea	Hydrothermal treatment, 180°C, 8h	CDs/TiO_2	Rhodamine B	94% in 120 min	.[199]
CA, urea	Hydrothermal treatment, 180°C, 5h	CDs/MoS_2 QDs/TiO_2 nanosheets	Rhodamine B	96.4% in 80 min	.[200]
CA, urea	Pyrolysis, 550°C, 3h	CDs alone	Methylene blue	90% at 1.015 kGy	.[201]

4.3 CA-CDs in organic solar cells

CA-CDs have been introduced in several types of organic photovoltaics (OPVs), such as dye-sensitized solar cells, perovskite-based solar cells and bulk heterojunction organic solar cells.[3] In all these systems, CA-CDs have been applied as photosensitizers, electron acceptors and hole acceptors, UV light down-converters, stabilizers and more, allowing to achieve solar cells with higher power conversion efficiency (PCE) and stability (Table 6).

Table 6. CA-CDs employed as components of photovoltaic devices.

CDs precursors	Synthesis method	Device structure	PCE, % increment due to CDs in ( )	Voc (V)	Jsc (mA cm^{-2}), % increment due to CDs in ( )	Effect in the application	Ref.
CA, 2,3-diaminonaphtalene	Solvothermal treatment (EtOH), 200°C, 9h	FTO/TiO_2@CDs:N-719:D149/Pt	8% (+0.7%)	0.73	14.7, (+1.2)	Extended absorption, photostability improvement	.[137]
CA, 2,3-diaminonaphtalene	Solvothermal treatment (EtOH), 200°C, 4h	FTO/TiO_2/TiO_2/$MAPbI_3$:CDs/Spiro-OMeTAD/Ag	19.38%, (+1.79%)	1.14	22.3, (+0.31)	Passivation of grain boundaries	.[202]
CA, 2-Imidazolidinethione	Hydrothermal treatment, 200°C	FTO/TiO_2@CDs/$MAPbI_3$/Spiro-MeOTAD/Au	18.87%, (+2.63%)	1.08	23.29, (+1.28)	Passivation of grain boundaries, electron extraction improvement	.[203]
CA, ammonium hydroxide	Pyrolysis, 200°C, 3h	FTO/TiO_2/TiO_2@CDs/electrolyte/Pt	0.79%	0.47	2.65	Electron extraction improvement	.[204]
CA, ammonium hydroxide	Pyrolysis, 200°C, 3h	FTO/TiO_2@CDs:ZnTSPc,I_2:LiI:DMPII:TBP/Pt	1.01%, (+0.67%)	0.47	4.20, (+2.23)	Enhanced charge separation	.[205]
CA, EDA	Hydrothermal treatment, 250°C, 5h	FTO/ZnOCDs@CDs:N719, KI:I_2/Pt	5.92%, (+4.12%)	0.67	2.34, (+1.56)	Enhanced charge separation	.[206]
CA, EDA	Hydrothermal treatment, 200°C, 5h	FTO/TiO_2/TiO_2:CDs/$MAPBCl_xI_{3-x}$/Spiro-OMeTAD/Au	16.4%, (+1.79%)	1.02	22.64, (+1.75)	Extended absorption, photostability improvement	.[207]
CA, EDA	Hydrothermal treatment, 230°C, 5h	ITO/NiO@CDs/N719, I^-:I^{3-}/Pt	9.85%, (+7.41%)	0.58	23.6, (+12.4)	Enhanced charge separation	.[208]
CA, EDA	Microwave irradiation, 750W, 8 min	ITO/PEIE/CDs/PTB7:PC_{71}BM/MoO_3/Ag	8.34%, (+0.91%)	0.76	16.7, (+2.4)	Electron extraction improvement	.[209]
CA, EDA	Hydrothermal treatment, 250°C, 10h	ITO/PEDOT:PSS/DR3TBDTT:PC_{71}BM/CDs/Al	7.78%, (+1.59%)	0.90	13.32, (+0.44)	Electron extraction improvement	.[210]
CA, EDA	Microwave irradiation, 750W, 8 min	ITO/PEIE/P3HT:PC_{60}BM:CDs/MoO_3/Ag	3.5%, (+0.8%)	0.65	8.0, (+1.1)	Enhanced charge separation	.[211]
CA, EDA	Hydrothermal treatment, 200°C, 5h	FTO/c-TiO2/m-TiO2/$MAPbI_3$:CDs/Spiro-OMeTAD/Ag	16.49%, (+3.70%)	1.08	20.66, (+1.31)	Passivation of grain boundaries, photosensitization	.[212]
CA, L-cysteine	Hydrothermal treatment, 200°C, 3h	ITO/Cs_2CO_3-CDs/P3HT:PCBM/V_2O_5/Au	3.17%, (+0.58%)	0.59	9.04, (+0.67)	Electron extraction improvement	.[213]
CA, NaOH	Hydrothermal treatment, 160°C, 10h	FTO/SnO_2@CDs/$MAPbI_3$/Spiro-OMeTAD/Au	19.2%, (+2.4%)	1.07	23.9, (+2.3)	Enhancement of charge transfer	.[214]
CA, Thiourea	Solvothermal treatment	ITO/PEDOT:PSS:CDs/$MAPbI_3$/PCBM:PCB/Ag	18.03%, (+2.62%)	1.01	22.60, (+0.95)	Hole extraction improvement	.[215]
CA, urea	Hydrothermal treatment, 200°C, 6h	FTO/TiO_2@CDs/Dye, I^-:I^{3-}/Pt	15.5%, (+7.7%)	1.06	22.2, (+13)	Increase of porosity, improved charge separation	.[216]
CA, urea	Microwave irradiation, 650W, 5 min	ITO/TiO_2/PC_{71}BM:PCDTBT/CDs/MoO_3/Ag	7.22%, (+1.29%)	0.87	14.71, (+1.22)	Hole extraction improvement	.[217]
CA, urea	Solvothermal treatment (DMF), 160°C, 6h	ITO/GO/CDs/$MAPbI_3$/PCBM/Ag	16.2 %, (+1.5%)	0.95	21.0, (+1.0)	Hole extraction improvement, photostability improvement	.[218]
CA, urea	Solvothermal treatment (DMF), 160°C, 6h	ITO/PTAA/$MAPbI_3$/CDs:SAM/C_{60}/Bphen/Ag	21.1%, (+2.5%)	1.10	23.2, (+1.83)	Electron extraction improvement, passivation of grain boundaries,	.[219]
CA, urea	Microwave irradiation, 450W, 2 min	FTO/TiO_2/TiO_2@CDs:N-719:I^-:I^{3-}/Pt	8.75%, (+4.30%)	0.71	18.13, (+7.87)	Extended absorption	.[220]
CA, β-Alanine	Microwave irradiation, 700W, 3 min	ITO/PEI:CDs/PTB7-Th:PC_{71}BM/MoO_3/Ag	9.49%, (+0.93%)	0.77	17.24, (+0.81)	Hole extraction improvement	.[221]

In *dye-sensitized solar cells (DSSCs)*, the presence of CA-CDs in the photoelectrode has proven to enhance the PCE through multiple mechanisms: i) the high number of CA-CDs charged groups provides better anchoring points for the adsorption of photosensitizer; ii) the light down-conversion due to the CA-CDs fluorescence increases the photon harvesting ability of the photosensitizer; iii) CA-CDs transport electrons from the photosensitizer LUMO level to electrode conductive band, counteracting charge recombination (Figure 16).[220] It is important to notice that in several works the preparation of the photoelectrode involves the annealing of CA-

CDs at temperatures between 230-500°C.[206,208,220] Plausibly, a harsh carbonization of their structure occurs at this step, creating extended aromatic domains that are beneficial for the electron transport ability observed.

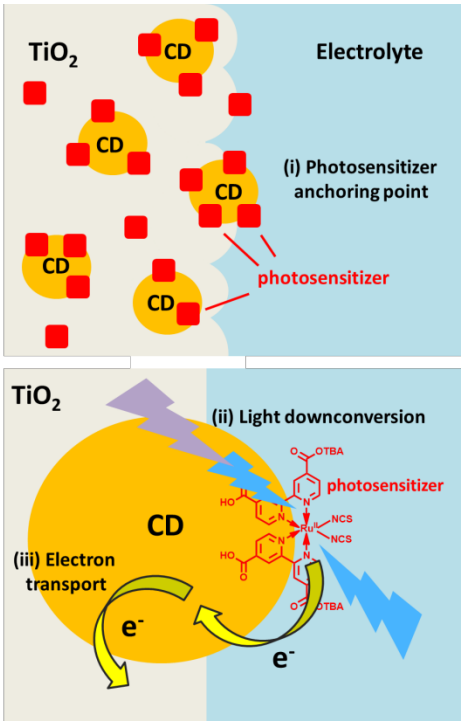

Figure 16. Roles of CA-CDs in the improvement of DSSC's photoelectrode performances.

In *perovskite-based solar cells (PSCs)*, the employment of CA-CDs has shown several benefits, in terms of both PCE enhancement and improved device stability. In the work of Jin et al., a CA-CDs layer was able to convert UV light to visible light, on one hand increasing the harvesting capability of the perovskite layer and, on the other, protecting its components from UV degradation.[207] Also when CA-CDs were introduced directly in the active layer by previously mixing them with the perovskite precursors the PCE of the devices was consistently improved.[202,212] The authors suggested that CA-CDs have a coordination effect at the grain boundaries. In fact, at the periphery of the perovskite crystals, uncoordinated I^- and Pb^{2+} act as

charge carrier recombination sites. Herein, the carboxylic groups, hydroxyl groups and amino-groups of CA-CDs are able to bind the uncoordinated ions, limiting their ability of trapping holes and electrons (Figure 17a). Moreover, the passivation with CA-CDs protects the perovskite from the contact with moisture, increasing the stability of the solar cell.[202] CA-CDs have been also exploited as a component of the charge transport layer. Impedance measurements showed that the presence of CA-CDs in the transport layer has a positive effect on the charge mobility, reflected in the increase short circuit current density (J_{sc}) of the cell.[203,207,214,218] In the work of Benedetti et al., CA-CDs were introduced as an additional hole transport layer between perovskite active layer and graphene oxide (GO) transport layer, showing that the CA-CDs layer can shift the work function of GO towards more negative values, improving its hole acceptor ability [218] Finally, the application of a CA-CDs/polyvinylpyrrolidone layer on the glass side of the PSC device could improve the stability of the cell and also increase the PCE, thanks to the CA-CDs conversion of UV light into blue-green light, suitable for the active layer absorption (Figure 17b).

In *bulk heterojunction organic solar cells (BHJ OSCs)*, the active layer consists of the blend of two organic components, designated to generate and separate electrons and holes upon light absorption. Most typically, modified fullerenes such as $PC_{60}BM$ or $PC_{71}BM$ are employed as efficient electron acceptors, while polythiophenes such as P3HT or PTB7-Th are popular low band gap electron donors. For example, Lim et Al. mixed different amounts of CA-CDs with P3HT and $PC_{60}BM$ for the preparation of the BHJ OSC active layer, obtaining an enhancement of Jsc and PCE in all the cases.[211] In other works, CA-CDs have been employed as components of the BHJ OSC electron transport layer.[209,210,213,221] Kang et al. prepared a device using PTB7-Th:$PC_{71}BM$ as photoactive layer and an ultra-thin polyethyleneimine (PEI) layer as electron

transport layer.[221] It is well known that the dipole-dipole organization of ultrathin PEI (<2 nm) can reduce the electrode surface work function and facilitate electrons extraction.[222] The authors synthesized CA-CDs by microwave irradiation of citric acid and β-Alanine and exploited them as addictive in the PEI layer. In this way, an increment of PCE was observed with respect to the case where PEI alone was employed. Therefore, they suggested that the zwitterionic nature of CA-CDs could improve the PEI layer dipole-dipole organization. Finally, Zhang et al. achieved a PCE improvement by exploiting CA-CDs as hole transport layer of an inverted BHJ OSC with structure ITO/TiO_2/PC_{71}BM:PCDTBT/CDs/MoO_3/Ag (Figure 17c and 17d).[217] The authors suggested that the CA-CDs interlayer can effectively bridge the separated islands of active layer to transport free charge carriers towards electrodes, reducing carrier recombination and improving charge mobility. Moreover, CA-CDs-mediated UV down-conversion enhanced the absorption of the active layer, further increasing the short-circuit current.

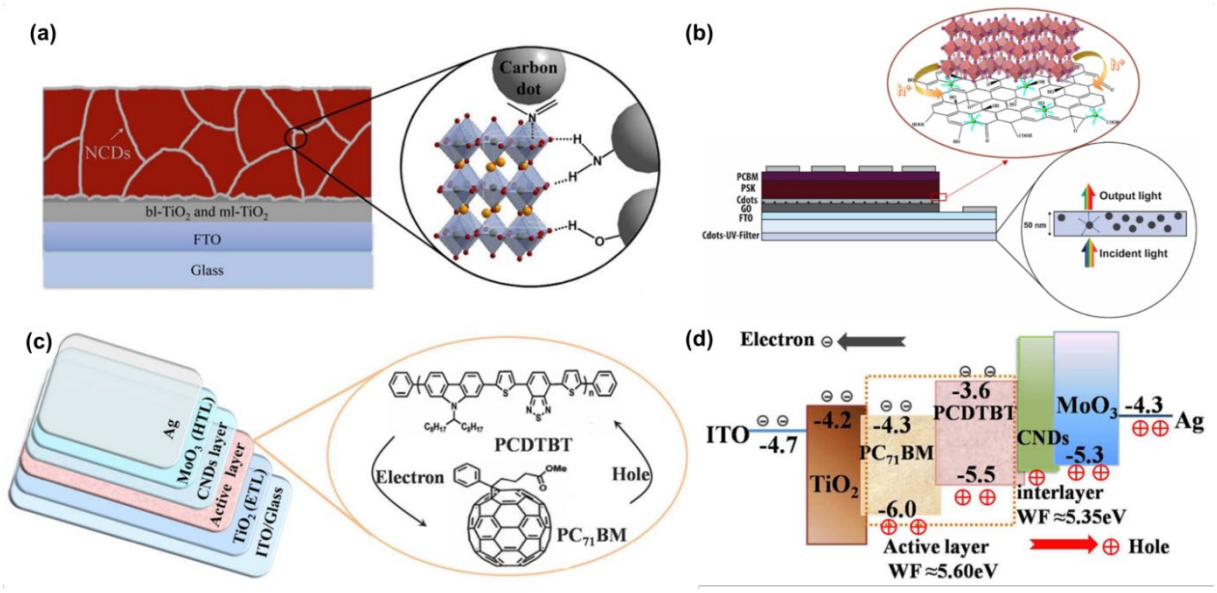

Figure 17. a) Schematic illustration of the proposed interaction between CA-CDs and perovskite grains. Reproduced from ref.[212] Copyright 2018, Springer Nature. b) Schematic of an inverted

planar device with CA-CDs incorporated at the interface between GO and perovskite, and a protective/down-shifting layer made of CA-CDs/PVP on the exterior side. Adapted from ref.[218] Copyright 2019, Elsevier. c) The device structure of the inverted BHJ-OSCs. d) Scheme of energy levels of the materials involved in inverted polymer solar cells. Adapted from ref.[217] Copyright 2016, American Chemical Society.

As described in this section and summarized in Table 6, the presence of CA-CDs can improve the performance of OPVs in very different ways through both physicochemical and electronic interactions with the other components. Nevertheless, in a consistent part of these studies CA-CDs were employed with little or no purification. Therefore, the heterogeneity of these materials does not allow the individuation of the organic structures contributing to the PCE enhancement. Beside the effect of the raw CA-CDs mixture on the OPV performances, it could be interesting to isolate and test the mixture components individually. In this way, the identification and optimization of key parameters could be pursued.

CONCLUSION

In summary, the thermal treatment of citric acid alone or jointly with other N-containing organic molecules can produce an incredible variety of molecular, oligomeric, polymeric and particle-like species with fluorescence properties. The nature of these species, their complexity and heterogeneity depends in first place on the choice of the synthetic precursors, but also on the reaction conditions, temperature and time. In here, by employing classification criteria based on the precursors, several CA-CDs systems of relevance have been discussed individually. We believe that this approach can provide a better understanding of the relationship between chemical structure and optical behavior of CA-CDs. Moreover, it helps to discern the differences

and the uniqueness among materials that are frequently grouped under a very general definition. In the second part of the article, a list of energy conversion applications of CA-CDs was presented. By circumscribing this list to the sole citric acid-based CDs, potentialities and limits of this specific class are outlined over the vast horizon of carbon dots materials. Undoubtedly, the results reported open the way to exciting possibilities in the field of energy conversion. Nevertheless, some issues should be addressed first. While it is ascertained that CA-CDs does not require a carbonization process in order to display fluorescence, higher temperatures could be crucial for the improvement of the CA-CDs charge-transfer ability. Thus, it remains to be seen if the excited states responsible for CA-CDs emission are the same involved in the charge transfer processes described in the context of several applications. If they are not, also the carbonization of alternative precursors into non-fluorescent nanoparticles could afford similar electronic activity. Another point that should be taken into account is that an improvement in the performance of heterojunctions could be not related necessarily to the CA-CDs electronic properties. Electrostatic and dipole interactions with metal or semiconductor surfaces can play an important role, by decreasing the material work function and facilitating electron injection. At the state of the art, these hypothesis have been scarcely explored and very little is known about the electronic phenomena taking place in CA-CDs. In order to obviate this problem, controllable syntheses followed by meticulous purification procedures are necessary, since they can provide materials with homogeneous structures and properties. Besides, more studies with a special focus on the relationship between CA-CDs structure and their electronic and optoelectronic properties are highly desirable. Only by improving the fundamental comprehension of these materials it will be possible to disclose their full potential for applications.

AUTHOR INFORMATION

Corresponding Author

* Lorenzo Vallan - Department of Molecular Engineering, Graduate School of Engineering, Kyoto University, Nishikyo-ku, Kyoto 615-8510, Japan. E-mail: vallan.lorenzo@gmail.com

* Hiroshi Imahori - Department of Molecular Engineering, Graduate School of Engineering, Kyoto University, Nishikyo-ku, Kyoto 615-8510, Japan and Institute for Integrated Cell-Material Sciences (WPI-iCeMS), Kyoto University, Sakyo-ku, Kyoto 606-8501, Japan. E-mail: imahori@scl.kyoto-u.ac.jp

Author Contributions

L.V. wrote the manuscript. H.I. supervised the work and corrected the manuscript.

ACKNOWLEDGMENT

This work was supported by the JSPS (KAKENHI Grant Numbers JP20H05831 (H.I.) and JP20H05832 (H.I.)). L. V. thanks JSPS Postdoctoral Fellowship for Research in Japan (PE21009).

REFERENCES

(1) Ji, C.; Zhou, Y.; Leblanc, R. M.; Peng, Z. Recent Developments of Carbon Dots in Biosensing : A Review. *ACS Sensors* **2020**, *5* (9), 2724–2741. https://doi.org/10.1021/acssensors.0c01556.

(2) Bayda, S.; Amadio, E.; Cailotto, S. Carbon Dots for Cancer Nanomedicine : A Bright Future. *Nanoscale Adv.* **2021**, *3*, 5183–5221. https://doi.org/10.1039/d1na00036e.

(3) Kim, A.; Dash, J. K.; Kumar, P.; Patel, R. Carbon-Based Quantum Dots for Photovoltaic Devices: A Review. *ACS Appl. Electron. Mater.* **2022**, *4* (1), 27–58. https://doi.org/10.1021/acsaelm.1c00783.

(4) Zhao, B.; Tan, Z. Fluorescent Carbon Dots: Fantastic Electroluminescent Materials for Light-Emitting Diodes. *Adv. Sci.* **2021**, *8* (7), 1–20. https://doi.org/10.1002/advs.202001977.

(5) Chen, B. Bin; Liu, M. L.; Huang, C. Z. Carbon Dot-Based Composites for Catalytic Applications. *Green Chem.* **2020**, *22* (13), 4034–4054. https://doi.org/10.1039/d0gc01014f.

(6) Cayuela, A.; Soriano, M. L.; Carrillo-Carriòn, C.; Valcárcel, M. Semiconductor and Carbon-Based Fluorescent Nanodots: The Need for Consistency. *Chem. Commun.* **2016**, *52*, 1311–1326. https://doi.org/10.1039/C5CC07754K.

(7) Xia, C.; Zhu, S.; Feng, T.; Yang, M.; Yang, B. Evolution and Synthesis of Carbon Dots: From Carbon Dots to Carbonized Polymer Dots. *Adv. Sci.* **2019**, *6* (23). https://doi.org/10.1002/advs.201901316.

(8) Demchenko, A. P.; Dekaliuk, M. O. The Origin of Emissive States of Carbon Nanoparticles Derived from Ensemble-Averaged and Single-Molecular Studies. *Nanoscale* **2016**, *8* (29), 14057–14069. https://doi.org/10.1039/C6NR02669A.

(9) Bhuyan, R.; Kommula, B.; Bhattacharyya, S. Specific Locations of Blue and Green-Emitting Units in Dual Emissive Carbon Dots and Their Reversible Emitting Properties Due to Switchable Inter-Chromophoric Interactions. *J. Colloid Interface Sci.* **2022**, *605*, 364–372. https://doi.org/10.1016/j.jcis.2021.07.119.

(10) Dekaliuk, M. O.; Viagin, O.; Malyukin, Y. V.; Demchenko, A. P. Fluorescent Carbon Nanomaterials: "Quantum Dots" or Nanoclusters? *Phys. Chem. Chem. Phys.* **2014**, *16* (30), 16075–16084. https://doi.org/10.1039/c4cp00138a.

(11) Hsu, Y. F.; Chen, Y. H.; Chang, C. W. The Spectral Heterogeneity and Size Distribution of the Carbon Dots Derived from Time-Resolved Fluorescence Studies. *Phys. Chem. Chem. Phys.* **2016**, *18* (43), 30086–30092. https://doi.org/10.1039/c6cp05813b.

(12) Zeng, Q.; Feng, T.; Tao, S.; Zhu, S.; Yang, B. Precursor-Dependent Structural Diversity in Luminescent Carbonized Polymer Dots (CPDs): The Nomenclature. *Light Sci. Appl.* **2021**, *10* (1). https://doi.org/10.1038/s41377-021-00579-6.

(13) Ren, J.; Malfatti, L.; Innocenzi, P. Citric Acid Derived Carbon Dots, the Challenge of Understanding the Synthesis-Structure Relationship. *J. Carbon Res.* **2020**, *7* (1), 2. https://doi.org/10.3390/c7010002.

(14) Nallayagari, A. R.; Sgreccia, E.; Pizzoferrato, R.; Cabibbo, M.; Kaciulis, S.; Bolli, E.; Pasquini, L.; Knauth, P.; Di Vona, M. L. Tuneable Properties of Carbon Quantum Dots by Different Synthetic Methods. *J. Nanostructure Chem.* **2021**, No. 0123456789. https://doi.org/10.1007/s40097-021-00431-8.

(15) Cailotto, S.; Mazzaro, R.; Enrichi, F.; Vomiero, A.; Selva, M.; Cattaruzza, E.; Cristofori, D.; Amadio, E.; Perosa, A. Design of Carbon Dots for Metal-Free Photoredox Catalysis. *ACS Appl. Mater. Interfaces* **2018**, *10* (47), 40560–40567. https://doi.org/10.1021/acsami.8b14188.

(16) Jiang, H.; Gu, J.; Zheng, X.; Liu, M.; Qiu, X.; Wang, L.; Li, W.; Chen, Z.; Ji, X.; Li, J. Defect-Rich and Ultrathin N Doped Carbon Nanosheets as Advanced Trifunctional Metal-Free Electrocatalysts for the ORR, OER and HER. *Energy Environ. Sci.* **2019**, *12* (1), 322–333. https://doi.org/10.1039/c8ee03276a.

(17) Yuan, F.; Wang, Z.; Li, X.; Li, Y.; Tan, Z.; Fan, L.; Yang, S. Bright Multicolor Bandgap Fluorescent Carbon Quantum Dots for Electroluminescent Light-Emitting Diodes. *Adv. Mater.* **2017**, *29* (3), 1–6. https://doi.org/10.1002/adma.201604436.

(18) Miao, X.; Qu, D.; Yang, D.; Nie, B.; Zhao, Y.; Fan, H.; Sun, Z. Synthesis of Carbon Dots with Multiple Color Emission by Controlled Graphitization and Surface Functionalization. *Adv. Mater.* **2018**, *30* (1), 1–8. https://doi.org/10.1002/adma.201704740.

(19) Yan, F.; Jiang, Y.; Sun, X.; Wei, J.; Chen, L.; Zhang, Y. Multicolor Carbon Dots with Concentration-Tunable Fluorescence and Solvent-Affected Aggregation States for White Light-Emitting Diodes. *Nano Res.* **2020**, *13* (1), 52–60. https://doi.org/10.1007/s12274-019-2569-3.

(20) Tian, Z.; Zhang, X.; Li, D.; Zhou, D.; Jing, P.; Shen, D.; Qu, S.; Zboril, R.; Rogach, A. L. Full-Color Inorganic Carbon Dot Phosphors for White-Light-Emitting Diodes. *Adv. Opt. Mater.* **2017**, *5* (19), 1–9. https://doi.org/10.1002/adom.201700416.

(21) Ding, H.; Wei, J. S.; Zhong, N.; Gao, Q. Y.; Xiong, H. M. Highly Efficient Red-Emitting Carbon Dots with Gram-Scale Yield for Bioimaging. *Langmuir* **2017**, *33* (44), 12635–12642. https://doi.org/10.1021/acs.langmuir.7b02385.

(22) Qu, D.; Sun, Z.; Zheng, M.; Li, J.; Zhang, Y.; Zhang, G.; Zhao, H.; Liu, X.; Xie, Z. Three Colors Emission from S,N Co-Doped Graphene Quantum Dots for Visible Light H2 Production and Bioimaging. *Adv. Opt. Mater.* **2015**, *3* (3), 360–367. https://doi.org/10.1002/adom.201400549.

(23) Zhang, X.; Zhang, Y.; Wang, Y.; Kalytchuk, S.; Kershaw, S. V.; Wang, Y.; Wang, P.;

Zhang, T.; Zhao, Y.; Zhang, H.; Cui, T.; Wang, Y.; Zhao, J.; Yu, W. W.; Rogach, A. L. Color-Switchable Electroluminescence of Carbon Dot Light-Emitting Diodes. *ACS Nano* **2013**, *7* (12), 11234–11241. https://doi.org/10.1021/nn405017q.

(24) Feng, M.; Liu, Y.; Wei, N.; Ma, S.; Li, Z.; Li, H.; Chen, S.; Liu, J.; Wang, D. Alumina Anchored CQDs/TiO2 Nanorods by Atomic Layer Deposition for Efficient Photoelectrochemical Water Splitting under Solar Light. *J. Mater. Chem. A* **2018**, *6* (37), 18293–18303. https://doi.org/10.1039/c8ta05092a.

(25) Zhou, Y.; Liyanage, P. Y.; Devadoss, D.; Rios Guevara, L. R.; Cheng, L.; Graham, R. M.; Chand, H. S.; Al-Youbi, A. O.; Bashammakh, A. S.; El-Shahawi, M. S.; Leblanc, R. M. Nontoxic Amphiphilic Carbon Dots as Promising Drug Nanocarriers across the Blood-Brain Barrier and Inhibitors of β-Amyloid. *Nanoscale* **2019**, *11* (46), 22387–22397. https://doi.org/10.1039/c9nr08194a.

(26) Lu, D.; Tang, Y.; Gao, J.; Chen, Y.; Wang, Q. Green Anhydrous Assembly of Carbon Dots via Solar Light Irradiation and Its Multi-Modal Sensing Performance. *Dye. Pigment.* **2019**, *165*, 287–293. https://doi.org/10.1016/j.dyepig.2019.02.037.

(27) Essner, J. B.; Kist, J. A.; Polo-parada, L.; Baker, G. A. Artifacts and Errors Associated with the Ubiquitous Presence of Fluorescent Impurities in Carbon Nanodots. *Chem. Mater.* **2018**, *30*, 1878–1887. https://doi.org/10.1021/acs.chemmater.7b04446.

(28) Chen, C. Y.; Tsai, Y. H.; Chang, C. W. Evaluation of the Dialysis Time Required for Carbon Dots by HPLC and the Properties of Carbon Dots after HPLC Fractionation. *New J. Chem.* **2019**, *43* (16), 6153–6159. https://doi.org/10.1039/c9nj00434c.

(29) Yao, X.; Wang, Y.; Li, F.; Dalluge, J. J.; Orr, G.; Hernandez, R.; Cui, Q.; Haynes, C. Unconventional Aliphatic Fluorophores Discovered as the Luminescence Origin in Citric Acid-Urea Carbon Dots. *Nanoscale* **2022**, *6*, 9516–9525. https://doi.org/10.1039/d2nr02361j.

(30) Arjun, S.; Trilochan, G.; Alka, G.; Anand, B.; Kumar, G. S.; Manoj, K. Origin of Excitation Dependent Fluorescence in Carbon Nanodots. *J. Phys. Chem. Lett.* **2016**, *7* (18), 3695–3702. https://doi.org/10.1021/acs.jpclett.6b01791.

(31) Anjali Devi, J. S.; Aparna, R. S.; Anjana, R. R.; Nebu, J.; Anju, S. M.; George, S. Solvent Effects: A Signature of J- And H-Aggregate of Carbon Nanodots in Polar Solvents. *J. Phys. Chem. A* **2019**, *123* (34), 7420–7429. https://doi.org/10.1021/acs.jpca.9b04568.

(32) Hinterberger, V.; Damm, C.; Haines, P.; Guldi, D. M.; Peukert, W. Purification and Structural Elucidation of Carbon Dots by Column Chromatography. *Nanoscale* **2019**, *11* (17), 8464–8474. https://doi.org/10.1039/c9nr01029g.

(33) Yuan, F.; Wang, Y. K.; Sharma, G.; Dong, Y.; Zheng, X.; Li, P.; Johnston, A.; Bappi, G.; Fan, J. Z.; Kung, H.; Chen, B.; Saidaminov, M. I.; Singh, K.; Voznyy, O.; Bakr, O. M.; Lu, Z. H.; Sargent, E. H. Bright High-Colour-Purity Deep-Blue Carbon Dot Light-Emitting Diodes via Efficient Edge Amination. *Nat. Photonics* **2020**, *14* (3), 171–176. https://doi.org/10.1038/s41566-019-0557-5.

(34) Ding, H.; Zhou, X.; Qin, B.; Zhou, Z.; Zhao, Y. Highly Fluorescent Near-Infrared Emitting Carbon Dots Derived from Lemon Juice and Its Bioimaging Application. *J. Lumin.* **2019**, *211* (March), 298–304. https://doi.org/10.1016/j.jlumin.2019.03.064.

(35) Zhi, B.; Yao, X.; Wu, M.; Mensch, A.; Cui, Y.; Deng, J.; Duchimaza-Heredia, J. J.; Trerayapiwat, K. J.; Niehaus, T.; Nishimoto, Y.; Frank, B. P.; Zhang, Y.; Lewis, R. E.; Kappel, E. A.; Hamers, R. J.; Fairbrother, H. D.; Orr, G.; Murphy, C. J.; Cui, Q.; Haynes, C. L. Multicolor Polymeric Carbon Dots: Synthesis, Separation and Polyamide-Supported Molecular Fluorescence. *Chem. Sci.* **2021**, *12* (7), 2441–2455. https://doi.org/10.1039/d0sc05743f.

(36) Wang, B.; Wang, S.; Wang, Y.; Lv, Y.; Wu, H.; Ma, X.; Tan, M. Highly Fluorescent Carbon Dots for Visible Sensing of Doxorubicin Release Based on Efficient Nanosurface Energy Transfer. *Biotechnol. Lett.* **2016**, *38* (1), 191–201. https://doi.org/10.1007/s10529-015-1965-3.

(37) Zhang, W.; Shi, L.; Liu, Y.; Meng, X.; Xu, H.; Xu, Y.; Liu, B.; Fang, X.; Li, H. B.; Ding, T. Supramolecular Interactions via Hydrogen Bonding Contributing to Citric-Acid Derived Carbon Dots with High Quantum Yield and Sensitive Photoluminescence. *RSC Adv.* **2017**, *7* (33), 20345–20353. https://doi.org/10.1039/c7ra02160g.

(38) Zhou, Y.; Mintz, K. J.; Oztan, C. Y.; Hettiarachchi, S. D.; Peng, Z.; Seven, E. S.; Liyanage, P. Y.; De La Torre, S.; Celik, E.; Leblanc, R. M. Embedding Carbon Dots in Superabsorbent Polymers for Additive Manufacturing. *Polymers (Basel).* **2018**, *10* (8), 1–12. https://doi.org/10.3390/polym10080921.

(39) Holá, K.; Sudolská, M.; Kalytchuk, S.; Nachtigallová, D.; Rogach, A. L.; Otyepka, M.; Zbořil, R. Graphitic Nitrogen Triggers Red Fluorescence in Carbon Dots. *ACS Nano* **2017**, *11* (12), 12402–12410. https://doi.org/10.1021/acsnano.7b06399.

(40) Kasprzyk, W.; Świergosz, T.; Bednarz, S.; Walas, K.; Bashmakova, N. V.; Bogdał, D. Luminescence Phenomena of Carbon Dots Derived from Citric Acid and Urea-a Molecular Insight. *Nanoscale* **2018**, *10* (29), 13889–13894. https://doi.org/10.1039/c8nr03602k.

(41) Song, Y.; Zhu, S.; Zhang, S.; Fu, Y.; Wang, L.; Zhao, X.; Yang, B. Investigation from Chemical Structure to Photoluminescent Mechanism: A Type of Carbon Dots from the Pyrolysis of Citric Acid and an Amine. *J. Mater. Chem. C* **2015**, *3* (23), 5976–5984. https://doi.org/10.1039/c5tc00813a.

(42) Vallan, L.; Urriolabeitia, E. P.; Ruipérez, F.; Matxain, J. M.; Canton-Vitoria, R.; Tagmatarchis, N.; Benito, A. M.; Maser, W. K. Supramolecular-Enhanced Charge Transfer within Entangled Polyamide Chains as the Origin of the Universal Blue Fluorescence of Polymer Carbon Dots. *J. Am. Chem. Soc.* **2018**, *140* (40), 12862–12869. https://doi.org/10.1021/jacs.8b06051.

(43) Schwan, J.; Ulrich, S.; Batori, V.; Ehrhardt, H.; Silva, S. R. P. Raman Spectroscopy on Amorphous Carbon Films. *J. Appl. Phys.* **1996**, *80* (440). https://doi.org/10.1063/1.362745.

(44) Reckmeier, C. J.; Schneider, J.; Xiong, Y.; Häusler, J.; Kasák, P.; Schnick, W.; Rogach, A. L. Aggregated Molecular Fluorophores in the Ammonothermal Synthesis of Carbon Dots. *Chem. Mater.* **2017**, *29* (24), 10352–10361. https://doi.org/10.1021/acs.chemmater.7b03344.

(45) Gude, V.; Das, A.; Chatterjee, T.; Mandal, P. K. Molecular Origin of Photoluminescence of Carbon Dots: Aggregation-Induced Orange-Red Emission. *Phys. Chem. Chem. Phys.* **2016**, *18* (40), 28274–28280. https://doi.org/10.1039/c6cp05321a.

(46) Khan, S.; Sharma, A.; Ghoshal, S.; Jain, S.; Hazra, M. K.; Nandi, C. K. Small Molecular Organic Nanocrystals Resemble Carbon Nanodots in Terms of Their Properties. *Chem. Sci.* **2017**, *9* (1), 175–180. https://doi.org/10.1039/c7sc02528a.

(47) Nandy, A.; Kumar, A.; Dwivedi, S.; Pal, S. K.; Panda, D. Connecting the Dots of Carbon Nanodots: Excitation (In)Dependency and White-Light Emission in One-Step. *J. Phys. Chem. C* **2019**, *123* (33), 20502–20511. https://doi.org/10.1021/acs.jpcc.9b02428.

(48) Samsul, A.; Othman, R.; Jabarullah, N. H. Preparation and Synthesis of Synthetic Graphite from Biomass Waste : A Review. *Syst. Rev. Pharm.* **2020**, *11* (2), 881–894.

(49) Dong, Y.; Shao, J.; Chen, C.; Li, H.; Wang, R.; Chi, Y.; Lin, X.; Chen, G. Blue Luminescent Graphene Quantum Dots and Graphene Oxide Prepared by Tuning the Carbonization Degree of Citric Acid. *Carbon N. Y.* **2012**, *50* (12), 4738–4743. https://doi.org/10.1016/j.carbon.2012.06.002.

(50) Ludmerczki, R.; Mura, S.; Carbonaro, C. M.; Mandity, I. M.; Carraro, M.; Senes, N.; Garroni, S.; Granozzi, G.; Calvillo, L.; Marras, S.; Malfatti, L.; Innocenzi, P. Carbon Dots from Citric Acid and Its Intermediates Formed by Thermal Decomposition. *Chem. - A Eur. J.* **2019**, *25* (51), 11963–11974. https://doi.org/10.1002/chem.201902497.

(51) Wang, S.; Chen, Z. G.; Cole, I.; Li, Q. Structural Evolution of Graphene Quantum Dots during Thermal Decomposition of Citric Acid and the Corresponding Photoluminescence. *Carbon N. Y.* **2015**, *82* (C), 304–313. https://doi.org/10.1016/j.carbon.2014.10.075.

(52) Dhenadhayalan, N.; Lin, K. C.; Suresh, R.; Ramamurthy, P. Unravelling the Multiple Emissive States in Citric-Acid-Derived Carbon Dots. *J. Phys. Chem. C* **2016**, *120* (2), 1252–

1261. https://doi.org/10.1021/acs.jpcc.5b08516.

(53) Manioudakis, J.; Victoria, F.; Thompson, C. A.; Brown, L.; Movsum, M.; Lucifero, R.; Naccache, R. Effects of Nitrogen-Doping on the Photophysical Properties of Carbon Dots. *J. Mater. Chem. C* **2019**, *7* (4), 853–862. https://doi.org/10.1039/c8tc04821e.

(54) Bagheri, Z.; Ehtesabi, H.; Rahmandoust, M.; Ahadian, M. M. New Insight into the Concept of Carbonization Degree in Synthesis of Carbon Dots to Achieve Facile Smartphone Based Sensing Platform. *Sci. Rep.* **2017**, No. August, 1–11. https://doi.org/10.1038/s41598-017-11572-8.

(55) Wang, P. J.; Li, C.; Liu, W.; Ren, Y.; Sun, X.; Pan, W.; Wang, J. The Selectivity of the Carboxylate Groups Terminated Carbon Dots Switched by Buffer Solutions for the Detection of Multi-Metal Ions. *Sensors Actuators B. Chem.* **2016**, *240*, 941–948. https://doi.org/10.1016/j.snb.2016.09.068.

(56) Martindale, B. C. M.; Hutton, G. A. M.; Caputo, C. A.; Reisner, E. Solar Hydrogen Production Using Carbon Quantum Dots and a Molecular Nickel Catalyst. *J. Am. Chem. Soc.* **2015**, *137* (18), 6018–6025. https://doi.org/10.1021/jacs.5b01650.

(57) Li, Z.; Wang, Y.; Ni, Y.; Kokot, S. A Rapid and Label-Free Dual Detection of Hg (II) and Cysteine with the Use of Fluorescence Switching of Graphene Quantum Dots. *Sensors Actuators B. Chem.* **2015**, *207*, 490–497. https://doi.org/10.1016/j.snb.2014.10.071.

(58) Xu, F.; Shi, H.; He, X.; Wang, K.; He, D.; Yan, L.; Ye, X.; Tang, J.; Shangguan, J.; Luo, L. Masking Agent-Free and Channel-Switch-Mode Simultaneous Sensing of Fe3+ and Hg2+ Using Dual-Excitation Graphene Quantum Dots. *Anal. (Cambridge, United Kingdom)* **2015**,

140 (12), 3925–3928. https://doi.org/10.1039/c5an00468c.

(59) Álvarez-diduk, R.; Orozco, J.; Merkoçi, A. Paper Strip-Embedded Graphene Quantum Dots : A Screening Device with a Smartphone Readout. *Sci. Rep.* **2017**, *7* (976). https://doi.org/10.1038/s41598-017-01134-3.

(60) Amjadi, M.; Manzoori, J. L.; Hallaj, T. Chemiluminescence of Graphene Quantum Dots and Its Application to the Determination of Uric Acid. *J. Lumin.* **2014**, *153*, 73–78. https://doi.org/10.1016/j.jlumin.2014.03.020.

(61) Huang, H.; Wang, B.; Chen, M.; Liu, M.; Leng, Y.; Liu, X.; Li, Y.; Liu, Z. Fluorescence Turn-on Sensing of Ascorbic Acid and Alkaline Phosphatase Activity Based on Graphene Quantum Dots. *Sensors Actuators B. Chem.* **2016**. https://doi.org/10.1016/j.snb.2016.05.080.

(62) Wu, Z.; Li, W.; Chen, J.; Yu, C. A Graphene Quantum Dot-Based Method for the Highly Sensitive and Selective Fl Uorescence Turn on Detection of Biothiols. *Talanta* **2014**, *119*, 538–543. https://doi.org/10.1016/j.talanta.2013.11.065.

(63) Huang, H.; Feng, Z.; Li, Y.; Liu, Z.; Zhang, L.; Ma, Y.; Tong, J. *Highly Sensitive Detection of Bisphenol A in Food Packaging Based on Graphene Quantum Dots and Peroxidase*; 2015. https://doi.org/10.1039/C4AY03080J.

(64) Qu, D.; Zheng, M.; Zhang, L.; Zhao, H.; Xie, Z.; Jing, X.; Haddad, R. E. Formation Mechanism and Optimization of Highly Luminescent N-Doped Graphene. *Sci. Rep.* **2014**, *4* (594), 1–11. https://doi.org/10.1038/srep05294.

(65) Zhou, S.; Sui, Y.; Zhu, X.; Sun, X.; Zhuo, S.; Li, H. Study and Comparison on Purification Methods of Multicolor Emission Carbon Dots. *Chem. - An Asian J.* **2021**, *16* (4), 348–354. https://doi.org/10.1002/asia.202001352.

(66) Nowak-wiczk, D. W. E. H. G. Thermal Behaviour of Citric Acid and Isomeric Aconitic Acids. *J. Therm. Anal. Calorim.* **2011**, *104*, 731–735. https://doi.org/10.1007/s10973-010-1015-2.

(67) Smith, E. L.; Abbott, A. P.; Ryder, K. S. Deep Eutectic Solvents (DESs) and Their Applications. *Chem. Rev.* **2014**, *114* (21), 11060–11082.

(68) Zholobak, N. M.; Popov, A. L.; Shcherbakov, A. B.; Popova, N. R.; Guzyk, M. M.; Antonovich, V. P.; Yegorova, A. V.; Scrypynets, Y. V.; Leonenko, I. I.; Baranchikov, A. Y.; Ivanov, V. K. Facile Fabrication of Luminescent Organic Dots by Thermolysis of Citric Acid in Urea Melt, and Their Use for Cell Staining and Polyelectrolyte Microcapsule Labelling. *Beilstein J. Nanotechnol.* **2016**, *7* (1), 1905–1917. https://doi.org/10.3762/BJNANO.7.182.

(69) Strauss, V.; Wang, H.; Delacroix, S.; Ledendecker, M.; Wessig, P. Carbon Nanodots Revised: The Thermal Citric Acid/Urea Reaction. *Chem. Sci.* **2020**, *11* (31), 8256–8266. https://doi.org/10.1039/d0sc01605e.

(70) Stachowska, J. D.; Murphy, A.; Mellor, C.; Fernandes, D.; Gibbons, E. N.; Krysmann, M. J.; Kelarakis, A.; Burgaz, E.; Moore, J.; Yeates, S. G. A Rich Gallery of Carbon Dots Based Photoluminescent Suspensions and Powders Derived by Citric Acid/Urea. *Sci. Rep.* **2021**, *11* (1), 1–14. https://doi.org/10.1038/s41598-021-89984-w.

(71) Crista, D. M. A.; da Silva, J. C. G. E.; da Silva, L. P. Evaluation of Different Bottom-up Routes for the Fabrication of Carbon Dots. *Nanomaterials* **2020**, *10* (7), 1–15. https://doi.org/10.3390/nano10071316.

(72) Simões, E. F. C.; Leitão, J. M. M.; da Silva, J. C. G. E. Carbon Dots Prepared from Citric Acid and Urea as Fluorescent Probes for Hypochlorite and Peroxynitrite. *Microchim. Acta* **2016**, *183* (5), 1769–1777. https://doi.org/10.1007/s00604-016-1807-6.

(73) Qu, S.; Liu, X.; Guo, X.; Chu, M.; Zhang, L.; Shen, D. Amplified Spontaneous Green Emission and Lasing Emission from Carbon Nanoparticles. *Adv. Funct. Mater.* **2014**, *24* (18), 2689–2695. https://doi.org/10.1002/adfm.201303352.

(74) Sendão, R. M. S.; Crista, D. M. A.; Afonso, A. C. P.; Martínez De Yuso, M. D. V.; Algarra, M.; Esteves Da Silva, J. C. G.; Pinto Da Silva, L. Insight into the Hybrid Luminescence Showed by Carbon Dots and Molecular Fluorophores in Solution. *Phys. Chem. Chem. Phys.* **2019**, *21* (37), 20919–20926. https://doi.org/10.1039/c9cp03730f.

(75) Pyne, A.; Layek, S.; Patra, A.; Sarkar, N. An Easy and Smart Way to Explore the Light-Emitting Responses of Carbon Dot and Doxorubicin Hydrochloride Assembly: White Light Generation and PH-Dependent Reversible Photoswitching. *J. Mater. Chem. C* **2019**, *7* (21), 6414–6425. https://doi.org/10.1039/c9tc01629e.

(76) Mukherjee, S.; Prasad, E.; Chadha, A. H-Bonding Controls the Emission Properties of Functionalized Carbon Nano-Dots. *Phys. Chem. Chem. Phys.* **2017**, *19* (10), 7288–7296. https://doi.org/10.1039/c6cp08889a.

(77) Zhao, P.; Jin, B.; Zhang, Q.; Peng, R. High-Quality Carbon Nitride Quantum Dots on

Photoluminescence: Effect of Carbon Sources. *Langmuir* **2021**, *37* (5), 1760–1767. https://doi.org/10.1021/acs.langmuir.0c02966.

(78) Song, X.; Guo, Q.; Cai, Z.; Qiu, J.; Dong, G. Synthesis of Multi-Color Fluorescent Carbon Quantum Dots and Solid State CQDs@SiO2 Nanophosphors for Light-Emitting Devices. *Ceram. Int.* **2019**, *45* (14), 17387–17394. https://doi.org/10.1016/j.ceramint.2019.05.299.

(79) Zhang, X.; Chen, C.; Peng, D.; Zhou, Y.; Zhuang, J.; Zhang, X.; Lei, B.; Liu, Y.; Hu, C. PH-Responsive Carbon Dots with Red Emission for Real-Time and Visual Detection of Amines. *J. Mater. Chem. C* **2020**, *8* (33), 11563–11571. https://doi.org/10.1039/d0tc02597f.

(80) Hu, T.; Wen, Z.; Thomas, T.; Wang, C.; Song, Q.; Yang, M.; Wang, C. Temperature-Controlled Spectral Tuning of Full-Color Carbon Dots and Their Strongly Fluorescent Solid-State Polymer Composites for Light-Emitting Diodes. *Nanoscale Adv.* **2019**, *1* (4), 1413–1420. https://doi.org/10.1039/c8na00329g.

(81) Zhou, J.; Yong, Y.; Zhang, C. A Low-Temperature Solid-Phase Method to Synthesize Highly Fluorescent Carbon Nitride Dots with Tunable Emission. *Chem. Commun.* **2013**, *49* (77), 8605–8607. https://doi.org/10.1039/c3cc42266f.

(82) Sciortino, A.; Mauro, N.; Buscarino, G.; Sciortino, L.; Popescu, R.; Schneider, R.; Giammona, G.; Gerthsen, D.; Cannas, M.; Messina, F. β-C3N4 Nanocrystals: Carbon Dots with Extraordinary Morphological, Structural, and Optical Homogeneity. *Chem. Mater.* **2018**, *30* (5), 1695–1700. https://doi.org/10.1021/acs.chemmater.7b05178.

(83) Freitas, F. S.; Gonçalves, A. S.; De Morais, A.; Benedetti, J. E.; Nogueira, A. F. Highly Luminescent S, N Co-Doped Graphene Quantum Dots with Broad Visible Absorption

Bands for Visible Light Photocatalyst. *J. Energy Sustain.* **2012**, No. 1, 11002–11003. https://doi.org/10.1039/c0xx00000x.

(84) Gu, S.; Hsieh, C. Te; Ashraf Gandomi, Y.; Li, J.; Yue, X. X.; Chang, J. K. Tailoring Fluorescence Emissions, Quantum Yields, and White Light Emitting from Nitrogen-Doped Graphene and Carbon Nitride Quantum Dots. *Nanoscale* **2019**, *11* (35), 16553–16561. https://doi.org/10.1039/c9nr05422g.

(85) Biswas, K.; Rathore, E.; Maji, K.; Rao, D.; Saha, B. Charge Transfer in the Heterostructure of CsPbBr3 Nanocrystals with Nitrogen-Doped Carbon Dots. *J. Phys. Chem. Lett.* **2020**, *11* (19), 8002–8007. https://doi.org/10.1021/acs.jpclett.0c02139.

(86) Vercelli, B.; Donnini, R.; Ghezzi, F.; Sansonetti, A.; Giovanella, U.; La Ferla, B. Nitrogen-Doped Carbon Quantum Dots Obtained Hydrothermally from Citric Acid and Urea: The Role of the Specific Nitrogen Centers in Their Electrochemical and Optical Responses. *Electrochim. Acta* **2021**, *387*, 138557. https://doi.org/10.1016/j.electacta.2021.138557.

(87) Dutta, A.; Trolles-Cavalcante, S. T. Y.; Cleetus, A.; Marks, V.; Schechter, A.; Webster, R. D.; Borenstein, A. Surface Modifications of Carbon Nanodots Reveal the Chemical Source of Their Bright Fluorescence. *Nanoscale Adv.* **2021**, *3* (3), 716–724. https://doi.org/10.1039/d0na00871k.

(88) Tomalia, D. A.; Klajnert-Maculewicz, B.; Johnson, K. A. M.; Brinkman, H. F.; Janaszewska, A.; Hedstrand, D. M. Non-Traditional Intrinsic Luminescence: Inexplicable Blue Fluorescence Observed for Dendrimers, Macromolecules and Small Molecular Structures Lacking Traditional/Conventional Luminophores. *Prog. Polym. Sci.* **2019**, *90*, 35–117.

https://doi.org/10.1016/j.progpolymsci.2018.09.004.

(89) Sun, M.; Han, Y.; Yuan, X.; Jing, P.; Zhang, L.; Zhao, J.; Zheng, Y. Efficient Full-Color Emitting Carbon-Dot-Based Composite Phosphors by Chemical Dispersion. *Nanoscale* **2020**, *12* (29), 15823–15831. https://doi.org/10.1039/d0nr02021d.

(90) Zhu, J.; Shao, H.; Bai, X.; Zhai, Y.; Yongsheng, Z.; Chen, X.; Pan, G.; Biao, D.; Xu, L.; Zhang, H.; Song, H. Modulation of the Photoluminescence in Carbon Dots through the Surface Modification: From Mechanism to White Light Emitting Diodes. *Nanotechnology* **2018**, *29*, 0–23.

(91) Guo, J.; Lu, Y.; Xie, A. Q.; Li, G.; Liang, Z. Bin; Wang, C. F.; Yang, X.; Chen, S. Yellow-Emissive Carbon Dots with High Solid-State Photoluminescence. *Adv. Funct. Mater.* **2022**, *32* (20), 1–11. https://doi.org/10.1002/adfm.202110393.

(92) Muzart, J. N,N -Dimethylformamide: Much More than a Solvent. *Tetrahedron* **2009**, *65* (40), 8313–8323. https://doi.org/10.1016/j.tet.2009.06.091.

(93) Serp, P.; Hernandez, M.; Richard, B.; Kalck, P. A Facile Route to Carbonylhalogenometal Complexes (M ، Rh , Ir , Ru , Pt) by Dimethylformamide Decarbonylation. *Eur. J. Inorg. Chem.* **2001**, No. 9, 2327–2336.

(94) Wan, Y.; Alterman, M.; Larhed, M.; Hallberg, A. Dimethylformamide as a Carbon Monoxide Source in Fast Palladium-Catalyzed Aminocarbonylations of Aryl Bromides. *J. Org. Chem.* **2002**, *67* (17), 6232–6235.

(95) Sun, S.; Zhang, L.; Jiang, K.; Wu, A.; Lin, H. Toward High-Efficient Red Emissive Carbon

Dots: Facile Preparation, Unique Properties, and Applications as Multifunctional Theranostic Agents. *Chem. Mater.* **2016**, *28* (23), 8659–8668. https://doi.org/10.1021/acs.chemmater.6b03695.

(96) Pan, L.; Sun, S.; Zhang, A.; Jiang, K.; Zhang, L.; Dong, C.; Huang, Q.; Wu, A.; Lin, H. Truly Fluorescent Excitation-Dependent Carbon Dots and Their Applications in Multicolor Cellular Imaging and Multidimensional Sensing. *Adv. Mater.* **2015**, *27* (47), 7782–7787. https://doi.org/10.1002/adma.201503821.

(97) Lu, H.; Xu, S.; Liu, J. One Pot Generation of Blue and Red Carbon Dots in One Binary Solvent System for Dual Channel Detection of Cr^{3+} and Pb^{2+} Based on Ion Imprinted Fluorescence Polymers. *ACS Sensors* **2019**, *4* (7), 1917–1924. https://doi.org/10.1021/acssensors.9b00886.a

(98) Wei, S.; Yin, X.; Li, H.; Du, X.; Zhang, L.; Yang, Q.; Yang, R. Multi-Color Fluorescent Carbon Dots: Graphitized Sp^2 Conjugated Domains and Surface State Energy Level Co-Modulate Band Gap Rather Than Size Effects. *Chem. - A Eur. J.* **2020**, *26* (36), 8129–8136. https://doi.org/10.1002/chem.202000763.

(99) Lan, X.; Ren, H.; Yang, X.; Wang, J.; Gao, P.; Zhang, Y. A Facile Microwave-Assisted Synthesis of Highly Crystalline Red Carbon Dots by Adjusting the Reaction Solvent for White Light-Emitting Diodes. *Nanotechnology* **2020**, *31* (21). https://doi.org/10.1088/1361-6528/ab71b6.

(100) Liang, W.; Wang, P.; Meziani, M. J.; Ge, L.; Yang, L.; Patel, A. K.; Morgan, S. O.; Sun, Y. P. On the Myth of "Red/near-IR Carbon Quantum Dots" from Thermal Processing of

Specific Colorless Organic Precursors. *Nanoscale Adv.* **2021**, *3* (14), 4186–4195. https://doi.org/10.1039/d1na00286d.

(101) Liang, W.; Ge, L.; Hou, X.; Ren, X.; Yang, L.; Bunker, C. E.; Overton, C. M.; Wang, P.; Sun, Y. Evaluation of Commercial "Carbon Quantum Dots" Sample on Origins of Red Absorption and Emission Features. *J. Carbon Res.* **2019**, *5* (4), 70.

(102) Chen, D.; Gao, H.; Chen, X.; Fang, G.; Yuan, S.; Yuan, Y. Excitation-Independent Dual-Color Carbon Dots : Surface-State Controlling and Solid-State Lighting Excitation-Independent Dual-Color Carbon Dots : Surface-State Controlling and Solid-State Lighting. *ACS Photonics* **2017**, *4* (9), 2352–2358. https://doi.org/10.1021/acsphotonics.7b00675.

(103) Cataldo, F.; Patanè, G.; Compagnini, G. Synthesis of HCN Polymer from Thermal Decomposition of Formamide. *J. Macromol. Sci. Part A Pure Appl. Chem.* **2009**, *46* (11), 1039–1048. https://doi.org/10.1080/10601320903245342.

(104) Ruiz-bermejo, M.; De, L.; Cristina, P.; Mateo-mart, E. A Comprehensive Review of HCN-Derived Polymers. *Processes* **2021**, *9* (4), 597.

(105) Zhu, S.; Meng, Q.; Wang, L.; Zhang, J.; Song, Y.; Jin, H.; Zhang, K.; Sun, H.; Wang, H.; Yang, B. Highly Photoluminescent Carbon Dots for Multicolor Patterning, Sensors, and Bioimaging. *Angew. Chemie - Int. Ed.* **2013**, *52* (14), 3953–3957. https://doi.org/10.1002/anie.201300519.

(106) Krysmann, M. J.; Kelarakis, A.; Dallas, P.; Giannelis, E. P. Formation Mechanism of Carbogenic Nanoparticles with Dual Photoluminescence Emission. *J. Am. Chem. Soc.* **2012**, *134* (2), 747–750. https://doi.org/10.1021/ja204661r.

(107) Deng, L.; Wang, X.; Kuang, Y.; Wang, C.; Luo, L.; Wang, F.; Sun, X. Development of Hydrophilicity Gradient Ultracentrifugation Method for Photoluminescence Investigation of Separated Non-Sedimental Carbon Dots. *Nano Res.* **2015**, *8* (9), 2810–2821. https://doi.org/10.1007/s12274-015-0786-y.

(108) Zhu, S.; Zhao, X.; Song, Y.; Lu, S.; Yang, B. Beyond Bottom-up Carbon Nanodots: Citric-Acid Derived Organic Molecules. *Nano Today* **2016**, *11* (2), 128–132. https://doi.org/10.1016/j.nantod.2015.09.002.

(109) Kasprzyk, W.; Bednarz, S.; Zmudzki, P.; Galica, M.; Bogdał, D. Novel Efficient Fluorophores Synthesized from Citric Acid. *RSC Adv.* **2015**, *5* (44), 34795–34799. https://doi.org/10.1039/c5ra03226a.

(110) Shi, L.; Yang, J. H.; Zeng, H. B.; Chen, Y. M.; Yang, S. C.; Wu, C.; Zeng, H.; Yoshihito, O.; Zhang, Q. Carbon Dots with High Fluorescence Quantum Yield: The Fluorescence Originates from Organic Fluorophores. *Nanoscale* **2016**, *8* (30), 14374–14378. https://doi.org/10.1039/c6nr00451b.

(111) Hoffmann, R. Interaction of Orbitals through Space and through Bonds. *Acc. Chem. Res.* **1970**, *4* (1), 1–9.

(112) Larson, C. L.; Tucker, S. A. Intrinsic Fluorescence of Carboxylate-Terminated Polyamido Amine Dendrimers. *Appl. Spectrosc.* **2001**, *55* (6), 679–683. https://doi.org/10.1366/0003702011952596.

(113) Sun, Y.; Cao, W.; Li, S.; Jin, S.; Hu, K.; Hu, L.; Huang, Y.; Gao, X.; Wu, Y.; Liang, X. Ultrabright and Multicolorful Fluorescence of Amphiphilic Polyethyleneimine Polymer

Dots for Efficiently Combined Imaging and Therapy. *Sci. Rep.* **2013**, *3* (3036). https://doi.org/10.1038/srep03036.

(114) Zhou, Q.; Cao, B.; Zhu, C.; Xu, S.; Gong, Y.; Yuan, W. Z.; Zhang, Y. Clustering-Triggered Emission of Nonconjugated Polyacrylonitrile. *Small* **2016**, *12* (47), 6586–6592. https://doi.org/10.1002/smll.201601545.

(115) Tao, S.; Zhou, C.; Kang, C.; Zhu, S.; Feng, T.; Zhang, S.; Ding, Z. Confined-Domain Crosslink-Enhanced Emission Effect in Carbonized Polymer Dots. *Light Sci. Appl.* **2022**, *11* (56). https://doi.org/10.1038/s41377-022-00745-4.

(116) Zhu, S.; Song, Y.; Shao, J.; Zhao, X.; Yang, B. Non-Conjugated Polymer Dots with Crosslink-Enhanced Emission in the Absence of Fluorophore Units. *Angew. Chemie - Int. Ed.* **2015**, *54* (49), 14626–14637. https://doi.org/10.1002/anie.201504951.

(117) Zhu, S.; Wang, L.; Zhou, N.; Zhao, X.; Song, Y.; Maharjan, S.; Zhang, J.; Lu, L.; Wang, H.; Yang, B. The Crosslink Enhanced Emission (CEE) in Non-Conjugated Polymer Dots: From the Photoluminescence Mechanism to the Cellular Uptake Mechanism and Internalization. *Chem. Commun.* **2014**, *50*, 13845–13848. https://doi.org/10.1039/c4cc05806b.

(118) Vallan, L.; Urriolabeitia, E. P.; Benito, A. M.; Maser, W. K. A Versatile Room-Temperature Method for the Preparation of Customized Fluorescent Non-Conjugated Polymer Dots. *Polymer (Guildf).* **2019**, *177* (April), 97–101. https://doi.org/10.1016/j.polymer.2019.05.041.

(119) Fluorescence Emission of Polyethyleneimine-Derived Polymer Dots and Its Application to

Detect Copper and Hypochlorite Ions. *ACS Appl. Mater. Interfaces* **2019**, *11* (35), 32489–32499. https://doi.org/10.1021/acsami.9b09545.

(120) Bhattacharyya, S.; Ehrat, F.; Urban, P.; Teves, R.; Wyrwich, R.; Döblinger, M.; Feldmann, J.; Urban, A. S.; Stolarczyk, J. K. Effect of Nitrogen Atom Positioning on the Trade-off between Emissive and Photocatalytic Properties of Carbon Dots. *Nat. Commun.* **2017**, *8* (1), 1–9. https://doi.org/10.1038/s41467-017-01463-x.

(121) Han, D.; Ma, M.; Han, Y.; Cui, Z.; Liang, Y.; Liu, X.; Li, Z.; Zhu, S.; Wu, S. Eco-Friendly Hybrids of Carbon Quantum Dots Modified MoS2 for Rapid Microbial Inactivation by Strengthened Photocatalysis. *ACS Sustain. Chem. Eng.* **2020**, *8* (1), 534–542. https://doi.org/10.1021/acssuschemeng.9b06045.

(122) Zhang, Y.; Xiao, J.; Zhuo, P.; Yin, H.; Fan, Y.; Liu, X.; Chen, Z. Carbon Dots Exhibiting Concentration-Dependent Full-Visible-Spectrum Emission for Light-Emitting Diode Applications. *ACS Appl. Mater. Interfaces* **2019**, *11* (49), 46054–46061. https://doi.org/10.1021/acsami.9b14472.

(123) Pandit, S.; Behera, P.; Sahoo, J.; De, M. In Situ Synthesis of Amino Acid Functionalized Carbon Dots with Tunable Properties and Their Biological Applications. *ACS Appl. Bio Mater.* **2019**, *2* (8), 3393–3403. https://doi.org/10.1021/acsabm.9b00374.

(124) Tao, S.; Song, Y.; Zhu, S.; Shao, J.; Yang, B. A New Type of Polymer Carbon Dots with High Quantum Yield: From Synthesis to Investigation on Fluorescence Mechanism. *Polymer (Guildf).* **2017**, *116*, 472–478. https://doi.org/10.1016/j.polymer.2017.02.039.

(125) Liu, L.; Mi, Z.; Wang, J.; Liu, Z.; Feng, F. A Label-Free Fluorescent Sensor Based on

Yellow-Green Emissive Carbon Quantum Dots for Ultrasensitive Detection of Congo Red and Cellular Imaging. *Microchem. J.* **2021**, *168* (March), 106420. https://doi.org/10.1016/j.microc.2021.106420.

(126) Huo, X.; Liu, L.; Bai, Y.; Qin, J.; Yuan, L.; Feng, F. Facile Synthesis of Yellowish-Green Emitting Carbon Quantum Dots and Their Applications for Phoxim Sensing and Cellular Imaging. *Anal. Chim. Acta* **2021**, No. xxxx, 338685. https://doi.org/10.1016/j.aca.2021.338685.

(127) Liu, Y.; Luo, S.; Wu, P.; Ma, C.; Wu, X.; Xu, M.; Li, W.; Liu, S. Hydrothermal Synthesis of Green Fluorescent Nitrogen Doped Carbon Dots for the Detection of Nitrite and Multicolor Cellular Imaging. *Anal. Chim. Acta* **2019**, *1090*, 133–142. https://doi.org/10.1016/j.aca.2019.09.015.

(128) An, Y.; Lin, X.; Zhou, Y.; Li, Y.; Zheng, Y.; Wu, C.; Xu, K.; Chai, X.; Liu, C. Red, Green, and Blue Light-Emitting Carbon Dots Prepared from o-Phenylenediamine. *RSC Adv.* **2021**, *11*, 26915–26919. https://doi.org/10.1039/d1ra02298a.

(129) Sato, R.; Iso, Y.; Isobe, T. Fluorescence Solvatochromism of Carbon Dot Dispersions Prepared from Phenylenediamine and Optimization of Red Emission. *Langmuir* **2019**, *35*, 15257–15266. https://doi.org/10.1021/acs.langmuir.9b02739.

(130) Song, L.; Cui, Y.; Zhang, C.; Hu, Z.; Liu, X. Microwave-Assisted Facile Synthesis of Yellow Fluorescent Carbon Dots from o-Phenylenediamine for Cell Imaging and Sensitive Detection of Fe3+ and H2O2. *RSC Adv.* **2016**, *6*, 17704–17712. https://doi.org/10.1039/C6RA02554D.

(131) Tan, A.; Yang, G.; Wan, X. Ultra-High Quantum Yield Nitrogen-Doped Carbon Quantum Dots and Their Versatile Application in Fluorescence Sensing, Bioimaging and Anti-Counterfeiting. *Spectrochim. Acta - Part A Mol. Biomol. Spectrosc.* **2021**, *253*, 119583. https://doi.org/10.1016/j.saa.2021.119583.

(132) Han, Z.; Nan, D.; Yang, H.; Sun, Q.; Pan, S.; Liu, H.; Hu, X. Carbon Quantum Dots Based Ratiometric Fluorescence Probe for Sensitive and Selective Detection of Cu2+ and Glutathione. *Sensors Actuators, B Chem.* **2019**, *298*, 126842. https://doi.org/10.1016/j.snb.2019.126842.

(133) Yang, X.; Zhang, Y.; Liu, W.; Gao, J.; Zheng, Y. Confined Synthesis of Phosphorus, Nitrogen Co-Doped Carbon Dots with Green Luminescence and Anion Recognition Performance. *Polyhedron* **2019**, *171*, 389–395. https://doi.org/10.1016/j.poly.2019.07.040.

(134) Singaravelu, C. M.; Deschanels, X.; Rey, C.; Causse, J. Solid-State Fluorescent Carbon Dots for Fluorimetric Sensing of Hg2+. *ACS Appl. Nano Mater.* **2021**, *4* (6), 6386–6397. https://doi.org/10.1021/acsanm.1c01400.

(135) Cai, W.; Zhang, T.; Xu, M.; Zhang, M.; Guo, Y.; Zhang, L.; Street, J.; Ong, W. J.; Xu, Q. Full Color Carbon Dots through Surface Engineering for Constructing White Light-Emitting Diodes. *J. Mater. Chem. C* **2019**, *7* (8), 2212–2218. https://doi.org/10.1039/c9tc00274j.

(136) Mondal, T. K.; Ghorai, U. K.; Saha, S. K. Dual-Emissive Carbon Quantum Dot-Tb Nanocomposite as a Fluorescent Indicator for a Highly Selective Visual Detection of Hg(II) in Water. *ACS Omega* **2018**, *3* (9), 11439–11446.

https://doi.org/10.1021/acsomega.8b01159.

(137) Riaz, R.; Ali, M.; Maiyalagan, T.; Anjum, A. S.; Lee, S.; Ko, M. J.; Jeong, S. H. Dye-Sensitized Solar Cell (DSSC) Coated with Energy down Shift Layer of Nitrogen-Doped Carbon Quantum Dots (N-CQDs) for Enhanced Current Density and Stability. *Appl. Surf. Sci.* **2019**, *483*, 425–431. https://doi.org/10.1016/j.apsusc.2019.03.236.

(138) Feng, T.; Zeng, Q.; Lu, S.; Yan, X.; Liu, J.; Tao, S.; Yang, M.; Yang, B. Color-Tunable Carbon Dots Possessing Solid-State Emission for Full-Color Light-Emitting Diodes Applications. *ACS Photonics* **2018**, *5* (2), 502–510. https://doi.org/10.1021/acsphotonics.7b01010.

(139) Do, S.; Kwon, W.; Rhee, S. W. Soft-Template Synthesis of Nitrogen-Doped Carbon Nanodots: Tunable Visible-Light Photoluminescence and Phosphor-Based Light-Emitting Diodes. *J. Mater. Chem. C* **2014**, *2* (21), 4221–4226. https://doi.org/10.1039/c4tc00090k.

(140) Zhang, T.; Zhao, F.; Li, L.; Qi, B.; Zhu, D.; Lü, J.; Lü, C. Tricolor White-Light-Emitting Carbon Dots with Multiple-Cores@Shell Structure for WLED Application. *ACS Appl. Mater. Interfaces* **2018**, *10* (23), 19796–19805. https://doi.org/10.1021/acsami.8b03529.

(141) Zhang, Y.; Yuan, R.; He, M.; Hu, G.; Jiang, J.; Xu, T.; Zhou, L.; Chen, W.; Xiang, W.; Liang, X. Multicolour Nitrogen-Doped Carbon Dots: Tunable Photoluminescence and Sandwich Fluorescent Glass-Based Light-Emitting Diodes. *Nanoscale* **2017**, *9* (45), 17849–17858. https://doi.org/10.1039/c7nr05363k.

(142) Zheng, J.; Wang, Y.; Zhang, F.; Yang, Y.; Liu, X.; Guo, K.; Wang, H.; Xu, B. Microwave-Assisted Hydrothermal Synthesis of Solid-State Carbon Dots with Intensive Emission for

White Light-Emitting Devices. *J. Mater. Chem. C* **2017**, *5* (32), 8105–8111. https://doi.org/10.1039/c7tc01701d.

(143) Yang, X.; Sui, L.; Wang, B.; Zhang, Y.; Tang, Z.; Yang, B.; Lu, S. Red-Emitting, Self-Oxidizing Carbon Dots for the Preparation of White LEDs with Super-High Color Rendering Index. *Sci. China Chem.* **2021**, *64* (9), 1547–1553. https://doi.org/10.1007/s11426-021-1033-6.

(144) Ding, Y.; Zheng, J.; Wang, J.; Yang, Y.; Liu, X. Direct Blending of Multicolor Carbon Quantum Dots into Fluorescent Films for White Light Emitting Diodes with an Adjustable Correlated Color Temperature. *J. Mater. Chem. C* **2019**, *7* (6), 1502–1509. https://doi.org/10.1039/c8tc04887h.

(145) Xie, Y.; Zhen, J.; Wang, Y.; Wang, J.; Yang, Y.; Liu, X.; Chen, Y. One-Step Hydrothermal Synthesis of Fluorescence Carbon Quantum Dots with High Product Yield and Quantum Yield. *Nanotechnology* **2019**, *30*.

(146) Zhang, F.; Feng, X.; Zhang, Y.; Yan, L.; Yang, Y.; Liu, X. Photoluminescent Carbon Quantum Dots as a Directly Film-Forming Phosphor towards White LEDs. *Nanoscale* **2016**, *8* (16), 8618–8632. https://doi.org/10.1039/c5nr08838k.

(147) Kim, T. H.; White, A. R.; Sirdaarta, J. P.; Ji, W.; Cock, I. E.; St John, J.; Boyd, S. E.; Brown, C. L.; Li, Q. Yellow-Emitting Carbon Nanodots and Their Flexible and Transparent Films for White LEDs. *ACS Appl. Mater. Interfaces* **2016**, *8* (48), 33102–33111. https://doi.org/10.1021/acsami.6b12113.

(148) Xie, Z.; Yin, Z.; Wu, Y.; Liu, C.; Hao, X.; Du, Q. White Light-Emitting Diodes Based on

Individual Polymerized Carbon Nanodots. *Sci. Rep.* **2017**, *7* (12146). https://doi.org/10.1038/s41598-017-12083-2.

(149) Sun, C.; Zhang, Y.; Kalytchuk, S.; Wang, Y.; Zhang, X.; Gao, W.; Zhao, J.; Cepe, K.; Zboril, R.; Yu, W. W.; Rogach, A. L. Down-Conversion Monochromatic Light-Emitting Diodes with the Color Determined by the Active Layer Thickness and Concentration of Carbon Dots. *J. Mater. Chem. C* **2015**, *3*, 6613–6615. https://doi.org/10.1039/C5TC01379H.

(150) Wang, Y.; Kalytchuk, S.; Zhang, Y.; Shi, H.; Kershaw, S. V. Thickness-Dependent Full-Color Emission Tunability in a Flexible Carbon Dot Ionogel. *J. Phys. Chem. Lett.* **2014**, *5* (8), 1412–1420.

(151) Zhou, D.; Zhai, Y.; Qu, S.; Li, D.; Jing, P.; Ji, W.; Shen, D.; Rogach, A. L. Electrostatic Assembly Guided Synthesis of Highly Luminescent Carbon-Nanodots @ BaSO 4 Hybrid Phosphors with Improved Stability. *Small* **2016**, *13* (6). https://doi.org/10.1002/smll.201602055.

(152) Kwon, W.; Lee, G.; Do, S.; Joo, T.; Rhee, S. Size-Controlled Soft-Template Synthesis of Carbon Nanodots toward Versatile Photoactive Materials. *Small* **2013**, *10* (3). https://doi.org/10.1002/smll.201301770.

(153) Wang, Y.; Zheng, J.; Wang, J.; Yang, Y.; Liu, X. Rapid Microwave-Assisted Synthesis of Highly Luminescent Nitrogen-Doped Carbon Dots for White Light-Emitting Diodes. *Opt. Mater. (Amst).* **2017**, *73*, 319–329. https://doi.org/10.1016/j.optmat.2017.08.032.

(154) Guo, H.; Liu, Z.; Shen, X.; Wang, L. One-Pot Synthesis of Orange Emissive Carbon Quantum Dots for All-Type High Color Rendering Index White Light-Emitting Diodes.

ACS Sustain. Chem. Eng. **2022**. https://doi.org/10.1021/acssuschemeng.2c00715.

(155) Wang, S.; Zhu, Z.; Chang, Y.; Wang, H.; Yuan, N.; Li, G.; Yu, D.; Jiang, Y. Ammonium Hydroxide Modulated Synthesis of High-Quality Fluorescent Carbon Dots for White LEDs with Excellent Color Rendering Properties. *Nanotechnology* **2016**, *27* (29), 1–9. https://doi.org/10.1088/0957-4484/27/29/295202.

(156) Chen, J.; Liu, W.; Mao, L. H.; Yin, Y. J.; Wang, C. F.; Chen, S. Synthesis of Silica-Based Carbon Dot/Nanocrystal Hybrids toward White LEDs. *J. Mater. Sci.* **2014**, *49* (21), 7391–7398. https://doi.org/10.1007/s10853-014-8413-y.

(157) Sun, Z.; Yan, F.; Xu, J.; Zhang, H.; Chen, L. Solvent-Controlled Synthesis Strategy of Multicolor Emission Carbon Dots and Its Applications in Sensing and Light-Emitting Devices. *Nano Res.* **2022**, *15* (1), 414–422. https://doi.org/10.1007/s12274-021-3495-8.

(158) Wang, X. F.; Wang, G. G.; Li, J. B.; Liu, Z.; Zhao, W. F.; Han, J. C. Towards High-Powered Remote WLED Based on Flexible White-Luminescent Polymer Composite Films Containing S, N Co-Doped Graphene Quantum Dots. *Chem. Eng. J.* **2018**, *336*, 406–415. https://doi.org/10.1016/j.cej.2017.12.056.

(159) Shen, C.; Zang, J.; Lou, Q.; Su, L.; Li, Z.; Liu, Z.; Dong, L.; Shan, C. In-Situ Embedding Carbon Dots in Trisodium Citrate Crystal Matrix for Tunable Solid-State Fluorescence. *Carbon N. Y.* **2018**, *136*, 359–368. https://doi.org/10.1016/j.carbon.2018.05.015.

(160) Lin, S.; Chen, M.; Wang, Z.; Zhang, Y.; Yuan, R.; Liang, X.; Xiang, W.; Zhou, Y. Construction of Full-Color Light-Emitting N-Based Carbon Nanodots and Their Efficient Solid-State Materials via Tape-Casting Technology for Warm WLED. *Chem. Eng. J.* **2017**,

324, 194–202. https://doi.org/10.1016/j.cej.2017.05.035.

(161) Xu, J.; Miao, Y.; Zheng, J.; Wang, H.; Yang, Y.; Liu, X. Carbon Dot-Based White and Yellow Electroluminescent Light Emitting Diodes with a Record-Breaking Brightness. *Nanoscale* **2018**, *10* (23), 11211–11221. https://doi.org/10.1039/c8nr01834k.

(162) Do, S.; Kwon, W.; Kim, Y.; Kang, S. R.; Lee, T.; Lee, T.; Rhee, S. N , S-Induced Electronic States of Carbon Nanodots Toward White Electroluminescence. *Adv. Opt. Mater.* **2016**, *4* (2), 276–284. https://doi.org/10.1002/adom.201500488.

(163) Xu, J.; Miao, Y.; Zheng, J.; Yang, Y.; Liu, X. Ultrahigh Brightness Carbon Dot – Based Blue Electroluminescent LEDs by Host – Guest Energy Transfer Emission Mechanism. *Adv. Opt. Mater.* **2018**, *6* (14). https://doi.org/10.1002/adom.201800181.

(164) Wang, F.; Chen, Y.; Liu, C.-Y.; Ma, D.-G. White Light-Emitting Devices Based on Carbon Dots' Electroluminescence. *Chem. Commun.* **2011**, *47* (12), 3502–3504. https://doi.org/10.1039/c0cc05391k.

(165) Kim, H. H.; Lee, Y. J.; Park, C.; Yu, S.; Won, S. O.; Seo, W. Bottom-Up Synthesis of Carbon Quantum Dots With High Performance Photo- and Electroluminescence. *Part. Part. Syst. Charact.* **2018**, *35* (7). https://doi.org/10.1002/ppsc.201800080.

(166) Hou, S.; Mahesh, K.; Quan, Q.; Hou, S.; Gangishetty, M. K.; Quan, Q.; Congreve, D. N. Efficient Blue and White Perovskite Light- Emitting Diodes via Manganese Doping Efficient Blue and White Perovskite Light-Emitting Diodes via Manganese Doping. *Joule* **2018**, *2* (11), 2421–2433. https://doi.org/10.1016/j.joule.2018.08.005.

(167) Liang, D.; Peng, Y.; Fu, Y.; Shearer, M. J.; Zhang, J.; Zhai, J. Color-Pure Violet-Light-Emitting Diodes Based on Layered Lead Halide Perovskite Nanoplates. *ACS Nano* **2016**, *10* (7), 6897–6904. https://doi.org/10.1021/acsnano.6b02683.

(168) Chen, Z.; Zhang, C.; Jiang, X.; Liu, M.; Xia, R.; Shi, T. High-Performance Color-Tunable Perovskite Light Emitting Devices through Structural Modulation from Bulk to Layered Film. *Adv. Mater.* **2017**, *29* (8). https://doi.org/10.1002/adma.201603157.

(169) Chen, T.; Yin, D.; Zhang, X.; Zhao, F.; Khaing, K. K.; Deng, L.; Huang, K.; Li, L.; Liu, J.; Zhang, Y. Fabrication of a Novel Carbon Quantum Dots-Modified 2D Heterojunction for Highly Efficient Sunlight Photocatalysis. *J. Alloys Compd.* **2019**, *806*, 761–773. https://doi.org/10.1016/j.jallcom.2019.07.215.

(170) Chen, Q.; Liu, Y.; Gu, X.; Li, D.; Zhang, D.; Zhang, D.; Huang, H.; Mao, B.; Kang, Z.; Shi, W. Carbon Dots Mediated Charge Sinking Effect for Boosting Hydrogen Evolution in Cu-In-Zn-S QDs/MoS2 Photocatalysts. *Appl. Catal. B Environ.* **2022**, *301* (August 2021). https://doi.org/10.1016/j.apcatb.2021.120755.

(171) Zhang, P.; Liu, H.; Li, X. Plasmonic CuCo/Carbon Dots: An Unconventional Photocatalyst Used for Photocatalytic Overall Water Splitting. *ACS Sustain. Chem. Eng.* **2020**, *8* (49), 17979–17987. https://doi.org/10.1021/acssuschemeng.0c05595.

(172) Zhang, P.; Zeng, G.; Song, T.; Huang, S.; Wang, T.; Zeng, H. Synthesis of a Plasmonic CuNi Bimetal Modified with Carbon Quantum Dots as a Non-Semiconductor-Driven Photocatalyst for Effective Water Splitting. *J. Catal.* **2019**, *369*, 267–275. https://doi.org/10.1016/j.jcat.2018.11.003.

(173) Jana, B.; Reva, Y.; Scharl, T.; Strauss, V.; Cadranel, A.; Guldi, D. M. Carbon Nanodots for All-in-One Photocatalytic Hydrogen Generation. *J. Am. Chem. Soc.* **2021**, *143*, 20122–20132. https://doi.org/10.1021/jacs.1c07049.

(174) Akbar, K.; Moretti, E.; Vomiero, A. Carbon Dots for Photocatalytic Degradation of Aqueous Pollutants : Recent Advancements. *Adv. Opt. Mater.* **2021**, *9*, 2100532. https://doi.org/10.1002/adom.202100532.

(175) Wu, S.; Zhou, R.; Chen, H.; Zhang, J.; Wu, P. Highly Efficient Oxygen Photosensitization of Carbon Dots: The Role of Nitrogen Doping. *Nanoscale* **2020**, *12* (9), 5543–5553. https://doi.org/10.1039/c9nr10986b.

(176) Li, J. F.; Zhong, C. Y.; Huang, J. R.; Chen, Y.; Wang, Z.; Liu, Z. Q. Carbon Dots Decorated Three-Dimensionally Ordered Macroporous Bismuth-Doped Titanium Dioxide with Efficient Charge Separation for High Performance Photocatalysis. *J. Colloid Interface Sci.* **2019**, *553*, 758–767. https://doi.org/10.1016/j.jcis.2019.06.077.

(177) Aghamali, A.; Khosravi, M.; Hamishehkar, H.; Modirshahla, N.; Behnajady, M. A. Synthesis and Characterization of High Efficient Photoluminescent Sunlight Driven Photocatalyst of N-Carbon Quantum Dots. *J. Lumin.* **2018**, *201*, 265–274. https://doi.org/10.1016/j.jlumin.2018.04.061.

(178) Yu, H.; Huang, J.; Jiang, L.; Shi, Y.; Yi, K.; Zhang, W. Enhanced Photocatalytic Tetracycline Degradation Using N-CQDs / OV-BiOBr Composites : Unraveling the Complementary Effects between N-CQDs and Oxygen Vacancy. *Chem. Eng. J.* **2020**, *402*. https://doi.org/10.1016/j.cej.2020.126187.

(179) Zhang, J.; Yuan, X.; Jiang, L.; Wu, Z.; Chen, X. Highly Efficient Photocatalysis toward Tetracycline of Nitrogen Doped Carbon Quantum Dots Sensitized Bi2WO6 Based on Interfacial Charge Transfer. *J. Colloid Interface Sci.* **2017**, *511*, 296–306. https://doi.org/10.1016/j.jcis.2017.09.083.

(180) Zhang, L. Y.; Han, Y. L.; Yang, J. J.; Deng, S. L.; Wang, B. Y. Construction and Photocatalysis of Carbon Quantum Dots/Layered Mesoporous Titanium Dioxide (CQDs/LM-TiO2) Composites. *Appl. Surf. Sci.* **2021**, *546* (October 2020), 149089. https://doi.org/10.1016/j.apsusc.2021.149089.

(181) Lee, H.; Anwer, H.; Park, J. Graphene Quantum Dots on Stainless-Steel Nanotubes for Enhanced Photocatalytic Degradation of Phenanthrene under Visible Light. *Chemosphere* **2020**, *246*. https://doi.org/10.1016/j.chemosphere.2019.125761.

(182) Wang, Y.; Niu, J.; Gao, X.; Zhang, Y. Synergetic Tuning of Photocatalytic Activity and Photostability of Ag3PO4 via Yttrium Doping, Carbon Quantum Dots and BiVO4 for Atenolol Degradation. *Appl. Surf. Sci.* **2020**, *533*, 147458. https://doi.org/10.1016/j.apsusc.2020.147458.

(183) Atkin, P.; Daeneke, T.; Wang, Y.; Carey, B. J.; Berean, K. J.; Clark, R. M.; Ou, J. Z.; Trinchi, A.; Cole, I. S.; Kalantar-Zadeh, K. 2D WS2/Carbon Dot Hybrids with Enhanced Photocatalytic Activity. *J. Mater. Chem. A* **2016**, *4* (35), 13563–13571. https://doi.org/10.1039/c6ta06415a.

(184) Zhang, X.; Li, Z.; Xu, S.; Ruan, Y. Carbon Quantum Dot-Sensitized Hollow TiO2spheres for High-Performance Visible Light Photocatalysis. *New J. Chem.* **2021**, *45* (19), 8693–

8700. https://doi.org/10.1039/d1nj00501d.

(185) Sharma, S.; Mehta, S. K.; Ibahdon, A. O.; Kansal, S. K. Fabrication of Novel Carbon Quantum Dots Modified Bismuth Oxide (α-Bi2O3/C-Dots): Material Properties and Catalytic Applications. *J. Colloid Interface Sci.* **2018**, *533*, 227–237. https://doi.org/10.1016/j.jcis.2018.08.056.

(186) Li, Q.; Lu, H.; Wang, X.; Hong, Z.; Fu, Z.; Liu, X.; Zhou, J. Visible-Light-Driven N and Fe Co-Doped Carbon Dots for Peroxymonosulfate Activation and Highly Efficient Aminopyrine Photodegradation. *Chem. Eng. J.* **2022**, *443* (April), 19–21. https://doi.org/10.1016/j.cej.2022.136473.

(187) Huo, P.; Guan, J.; Zhou, M.; Ma, C.; Liu, X.; Yan, Y.; Yuan, S. Carbon Quantum Dots Modified CdSe Loaded Reduced Graphene Oxide for Enhancing Photocatalytic Activity. *J. Ind. Eng. Chem.* **2017**, *50*, 147–154. https://doi.org/10.1016/j.jiec.2017.02.008.

(188) Chen, Y.; Lu, Q.; Yan, X.; Mo, Q.; Chen, Y.; Liu, B.; Teng, L.; Xiao, W.; Ge, L.; Wang, Q. Enhanced Photocatalytic Activity of the Carbon Quantum Dot-Modified BiOI Microsphere. *Nanoscale Res. Lett.* **2016**, *11* (1), 1–7. https://doi.org/10.1186/s11671-016-1262-7.

(189) Hong, Y.; Meng, Y.; Zhang, G.; Yin, B.; Zhao, Y.; Shi, W.; Li, C. Facile Fabrication of Stable Metal-Free CQDs/g-C3N4 Heterojunctions with Efficiently Enhanced Visible-Light Photocatalytic Activity. *Sep. Purif. Technol.* **2016**, *171*, 229–237. https://doi.org/10.1016/j.seppur.2016.07.025.

(190) Zhu, W.; Li, X. Graphene Quantum Dots / LaCoO3 / Attapulgite Heterojunction Photocatalysts with Improved Photocatalytic Activity. *Appl. Phys. A* **2017**, *123*.

https://doi.org/10.1007/s00339-017-0907-4.

(191) Jiang, R.; Wu, D.; Lu, G.; Yan, Z.; Liu, J. Modified 2D-2D ZnIn2S4/BiOCl van Der Waals Heterojunctions with CQDs : Accelerated Charge Transfer and Enhanced Photocatalytic Activity under Vis- and NIR-Light. *Chemosphere* **2019**, *227*, 82–92. https://doi.org/10.1016/j.chemosphere.2019.04.038.

(192) Wang, Y.; Chen, B. Bin; Gao, Y. T.; Jiang, L.; Lv, J.; Chang, S.; Qian, R. C.; Li, D. W. Carbon Dots Induced In-Situ Formation of Porous Europium Micro-Networks with Enhanced Photocatalysis. *J. Colloid Interface Sci.* **2022**, *606*, 600–606. https://doi.org/10.1016/j.jcis.2021.08.057.

(193) Wang, W.; Zeng, Z.; Zeng, G.; Zhang, C.; Xiao, R. Sulfur Doped Carbon Quantum Dots Loaded Hollow Tubular G-C3N4 as Novel Photocatalyst for Destruction of Escherichia Coli and Tetracycline Degradation under Visible Light. *Chem. Eng. J.* **2019**, *378*. https://doi.org/10.1016/j.cej.2019.122132.

(194) Chattopadhyay, S.; Mishra, M. K.; De, G. Functionalized C@TiO2 Hollow Spherical Architecture for Multifunctional Applications. *Dalt. Trans.* **2016**, *45* (12), 5111–5121. https://doi.org/10.1039/c5dt05011a.

(195) Zhang, J.; Zhang, X.; Ren, Z.; Yang, L.; Tang, Y.; Ma, Y.; Cui, Y.; Gao, B.; Chu, P. K. Influence of Photon Reabsorption on the Optical and Catalytic Properties of Carbon Nanodots/Titanium Oxide Composites. *Appl. Phys. Lett.* **2022**, *120* (21). https://doi.org/10.1063/5.0093878.

(196) Zhao, J.; He, Q.; Zhang, X.; Guo, X.; Song, Q.; Liu, Y.; Yao, B. Fabrication of CQDs /

Bi5Nb3O15 Nanocomposites for Photocatalytic Degradation of Veterinary Pharmaceutical Sarafloxacin. *Catal. Today* **2020**, *355*, 716–726. https://doi.org/10.1016/j.cattod.2019.05.006.

(197) Liu, X. R.; Sheng, X. X.; Yuan, X. Y.; Liu, J. K.; Sun, X. W.; Yang, X. H. Research on Correlation between Corrosion Resistance and Photocatalytic Activity of Molybdenum Zinc Oxide Modified by Carbon Quantum Dots Pigments. *Dye. Pigment.* **2020**, *175* (December 2019), 108148. https://doi.org/10.1016/j.dyepig.2019.108148.

(198) Li, D.; Huang, J.; Li, R.; Chen, P.; Chen, D.; Cai, M.; Liu, H.; Feng, Y.; Lv, W.; Liu, G. Synthesis of a Carbon Dots Modified G-C3N4/SnO2 Z-Scheme Photocatalyst with Superior Photocatalytic Activity for PPCPs Degradation under Visible Light Irradiation. *J. Hazard. Mater.* **2021**, *401*, 123257. https://doi.org/10.1016/j.jhazmat.2020.123257.

(199) Sun, X.; Li, H. J.; Ou, N.; Lyu, B.; Gui, B.; Tian, S.; Qian, D.; Wang, X.; Yang, J. Visible-Light Driven TiO2 Photocatalyst Coated with Graphene Quantum Dots of Tunable Nitrogen Doping. *Molecules* **2019**, *24* (2). https://doi.org/10.3390/molecules24020344.

(200) Zhang, Q.; Zhao, H.; Dong, Y.; Zhu, X.; Liu, X.; Li, H. A Novel Ternary MQDs/NCDs/TiO2nanocomposite That Collaborates with Activated Persulfate for Efficient RhB Degradation under Visible Light Irradiation. *New J. Chem.* **2021**, *45* (3), 1327–1338. https://doi.org/10.1039/d0nj05640e.

(201) Ye, Q.; Yang, M.; Li, W.; Dong, Z.; Qi, W.; Zhao, L. Heterogeneous Irradiation System: Enhanced Degradation of Methylene Blue by Electron Beam Irradiation Combined with Graphite Carbon Nitride/Carbon Nanodots. *Environ. Sci. Pollut. Res.* **2022**, No.

0123456789. https://doi.org/10.1007/s11356-022-19934-0.

(202) Guo, Q.; Yuan, F.; Zhang, B.; Zhou, S.; Zhang, J.; Bai, Y.; Fan, L.; Hayat, T.; Alsaedi, A.; Tan, Z. Passivation of the Grain Boundaries of CH3NH3PbI3 Using Carbon Quantum Dots for Highly Efficient Perovskite Solar Cells with Excellent Environmental Stability. *Nanoscale* **2019**, *11* (1), 115–124. https://doi.org/10.1039/c8nr08295b.

(203) Sidhik, S.; Velusamy, J.; De la Rosa, E.; Pérez-García, S. A.; Ramos-Ortiz, G.; López-Luke, T. Role of Carbon Nanodots in Defect Passivation and Photo-Sensitization of Mesoscopic-TiO 2 for Application in Perovskite Solar Cells. *Carbon N. Y.* **2019**, *146*, 388–398. https://doi.org/10.1016/j.carbon.2019.01.105.

(204) Wang, H.; Sun, P.; Cong, S.; Wu, J.; Gao, L.; Wang, Y.; Dai, X.; Yi, Q.; Zou, G. Nitrogen-Doped Carbon Dots for "Green" Quantum Dot Solar Cells. *Nanoscale Res. Lett.* **2016**, *11* (1), 1–6. https://doi.org/10.1186/s11671-016-1231-1.

(205) Ghadari, R.; Saei, P. S.; Sabri, A.; Ghasemi, Z.; Kong, F. Enhanced Phthalocyanine-Sensitized Solar Cell Efficiency via Cooperation of Nitrogen-Doped Carbon Dots. *J. Clean. Prod.* **2020**, *268*, 122236. https://doi.org/10.1016/j.jclepro.2020.122236.

(206) Efa, M. T.; Imae, T. Effects of Carbon Dots on ZnO Nanoparticle-Based Dye-Sensitized Solar Cells. *Electrochim. Acta* **2019**, *303*, 204–210. https://doi.org/10.1016/j.electacta.2019.02.012.

(207) Jin, J.; Chen, C.; Li, H.; Cheng, Y.; Xu, L.; Dong, B.; Song, H.; Dai, Q. Enhanced Performance and Photostability of Perovskite Solar Cells by Introduction of Fluorescent Carbon Dots. *ACS Appl. Mater. Interfaces* **2017**, *9* (16), 14518–14524.

https://doi.org/10.1021/acsami.7b02242.

(208) Etefa, H. F.; Imae, T.; Yanagida, M. Enhanced Photosensitization by Carbon Dots Co-Adsorbing with Dye on p-Type Semiconductor (Nickel Oxide) Solar Cells. *ACS Appl. Mater. Interfaces* **2020**, *12* (16), 18596–18608. https://doi.org/10.1021/acsami.0c02413.

(209) Lim, H.; Liu, Y.; Kim, H. Y.; Son, D. I. Facile Synthesis and Characterization of Carbon Quantum Dots and Photovoltaic Applications. *Thin Solid Films* **2018**, *660* (December 2017), 672–677. https://doi.org/10.1016/j.tsf.2018.04.019.

(210) Zhang, H.; Zhang, Q.; Li, M.; Kan, B.; Ni, W.; Wang, Y.; Yang, X.; Du, C.; Wan, X.; Chen, Y. Investigation of the Enhanced Performance and Lifetime of Organic Solar Cells Using Solution-Processed Carbon Dots as the Electron Transport Layers. *J. Mater. Chem. C* **2015**, *3* (48), 12403–12409. https://doi.org/10.1039/c5tc02957k.

(211) Lim, H.; Lee, K. S.; Liu, Y.; Kim, H. Y.; Son, D. I. Photovoltaic Performance of Inverted Polymer Solar Cells Using Hybrid Carbon Quantum Dots and Absorption Polymer Materials. *Electron. Mater. Lett.* **2018**, *14* (5), 581–586. https://doi.org/10.1007/s13391-018-0064-8.

(212) Wang, Y.; Zhang, J.; Chen, S.; Zhang, H.; Li, L.; Fu, Z. Surface Passivation with Nitrogen-Doped Carbon Dots for Improved Perovskite Solar Cell Performance. *J. Mater. Sci.* **2018**, *53* (12), 9180–9190. https://doi.org/10.1007/s10853-018-2190-y.

(213) Yang, H.; Dong, Y.; Wang, X.; Khoo, S.; Liu, B.; Li, C. M. Graphene Quantum Dots-Incorporated Cathode Buffer for Improvement of Inverted Polymer Solar Cells. *Sol. Energy Mater. Sol. Cells* **2013**, *117*, 214–218. https://doi.org/10.1016/j.solmat.2013.05.060.

(214) Zhou, Y.; Yang, S.; Yin, X.; Han, J.; Tai, M.; Zhao, X.; Chen, H.; Gu, Y.; Wang, N.; Lin, H. Enhancing Electron Transport via Graphene Quantum Dot/SnO2 Composites for Efficient and Durable Flexible Perovskite Photovoltaics. *J. Mater. Chem. A* **2019**, *7* (4), 1878–1888. https://doi.org/10.1039/c8ta10168j.

(215) Li, Z.; Liu, C.; Zhang, X.; Guo, J.; Cui, H.; Shen, L.; Bi, Y.; Guo, W. Using Easily Prepared Carbon Nanodots to Improve Hole Transport Capacity of Perovskite Solar Cells. *Mater. Today Energy* **2019**, *12*, 161–167. https://doi.org/10.1016/j.mtener.2019.01.002.

(216) Padmanathan, S.; Prakasam, A. Design and Fabrication of Hybrid Carbon Dots/Titanium Dioxide (CDs/TiO2) Photoelectrodes for Highly Efficient Dye-Sensitized Solar Cells. *J. Mater. Sci. Mater. Electron.* **2020**, *31* (4), 3492–3499. https://doi.org/10.1007/s10854-020-02897-8.

(217) Zhang, X.; Li, Z.; Zhang, Z.; Li, S.; Liu, C.; Guo, W.; Shen, L.; Qu, S.; Ruan, S. Efficiency Improvement of Organic Solar Cells via Introducing Combined Anode Buffer Layer To Facilitate Hole Extraction. *J. Phys. Chem. C* **2016**, *120* (26), 13954–13962. https://doi.org/10.1021/acs.jpcc.6b03697.

(218) Benetti, D.; Jokar, E.; Yu, C. H.; Fathi, A.; Zhao, H.; Vomiero, A.; Wei-Guang Diau, E.; Rosei, F. Hole-Extraction and Photostability Enhancement in Highly Efficient Inverted Perovskite Solar Cells through Carbon Dot-Based Hybrid Material. *Nano Energy* **2019**, *62*, 781–790. https://doi.org/10.1016/j.nanoen.2019.05.084.

(219) Li, Z.; Guo, J.; Li, Z.; Han, W.; Ren, G.; Liu, C.; Shen, L.; Guo, W. Incorporating Self-Assembled Silane-Crosslinked Carbon Dots into Perovskite Solar Cells to Improve

Efficiency and Stability. *J. Mater. Chem. A* **2020**, *8* (11), 5629–5637. https://doi.org/10.1039/d0ta00123f.

(220) Shejale, K. P.; Jaiswal, A.; Kumar, A.; Saxena, S.; Shukla, S. Nitrogen Doped Carbon Quantum Dots as Co-Active Materials for Highly Efficient Dye Sensitized Solar Cells. *Carbon N. Y.* **2021**, *183*, 169–175. https://doi.org/10.1016/j.carbon.2021.06.090.

(221) Kang, R.; Park, S.; Jung, Y. K.; Lim, D. C.; Cha, M. J.; Seo, J. H.; Cho, S. High-Efficiency Polymer Homo-Tandem Solar Cells with Carbon Quantum-Dot-Doped Tunnel Junction Intermediate Layer. *Adv. Energy Mater.* **2018**, *8* (10). https://doi.org/10.1002/aenm.201702165.

(222) Zhou, Y.; Fuentes-Hernandez, C.; Won Shim, J.; Khan, T. M.; Kippelen, B. High Performance Polymeric Charge Recombination Layer for Organic Tandem Solar Cells. *Energy Environ. Sci.* **2012**, *5*, 9827–9832. https://doi.org/10.1039/c2ee23294d.